UiO : Department of Geosciences
University of Oslo

Implementation and Evaluation of a Wet-Avalanche Activity Index in the seNorge Snow Model

Torkjell Holm Brenna

Master's Thesis, Spring 2020

Implementation and Evaluation of a Wet-Avalanche Activity Index in the seNorge Snow Model

Torkjell Holm Brenna

This master's thesis is submitted under the master's programme *Geosciences*, with programme option *Geohazards and Geomechanics*. The scope of the thesis is 60 credits.

Department of Geosciences

Faculty of Mathematics and Natural Sciences

UNIVERSITY OF OSLO

June 2020

Abstract

Assessing wet snow stability is a difficult task. The processes that lead to wet-snow instability are complex, and the strength of a snowpack can decrease within minutes after water infiltrates the snow. This has caused great challenges in forecasting wet-snow avalanches as the critical conditions for release are difficult to assess. In addition, the conditions where wet-snow avalanches can trigger often only exist for a short period of time.

In a study in Switzerland, a liquid water content index (LWC index) that improves the reliability of wet-snow avalanche forecasts was created. This study found that an average volumetric liquid water content of the entire snowpack at 3% indicates the onset of wet-snow avalanche activity. To calculate the index, the authors used the 1-D snow cover model SNOWPACK, which requires measured mass and energy balance values.

In Norway, the less demanding seNorge model is run to produce maps of snow cover with a 1x1 km resolution. This model only requires air temperature and precipitation to produce information about the snow water equivalent and snow depth. We implemented the LWC index in the seNorge model to attempt to reproduce the results from Switzerland. The index was compared to observed wet-snow avalanche activity from two regions, Tyin and Tromsø.

We could only reproduce parts of the findings from Switzerland. The index agreed well with wet-snow avalanche activity when temperatures were high and little to no precipitation was registered. Once continuous precipitation was recorded the forecasting performance was poor. We hypothesised that this was caused by a problem with the algorithm used for calculating shortwave radiation in the model. There were also difficulties with correctly modeling the type of precipitation. This was presumably caused by the dependence of temperature on altitude, as the difference in altitude between the location of the input data and the avalanche was sometimes large.

To be able to use the LWC index for forecasting purposes in Norway a solution for indicating wet-snow avalanche activity correctly at times with precipitation is necessary. However, with further work, the tool shows promise for better predictions of wet-snow avalanches in the future.

Acknowledgements

First and foremost, I want to thank my supervisors Karsten Müller (UiO and NVE) and Tuomo Saloranta (NVE) for making this master thesis a reality. I am grateful for the support given regarding valuable feedback and time invested, especially with all the help in setting up and using the seNorge model.

Further, I would like to thank Stian Langeland and Cesar Vera from Wyssen Avalanche Control for providing the Tyin avalanche inventory and for running the SNOWPACK model over that area for me. I would also like to thank Markus Eckstorfer from NORCE for providing the avalanche inventory over Troms county. Without these data, the thesis would not have been possible.

I would especially like to thank my family for moral support during my entire studies. My father has always helped me when needed. A special thanks to my brother, Borgar, for proof-reading this thesis.

Lastly, I would like to show my appreciation to my girlfriend. You have been supporting and helping me throughout the entire process. A process that was at times very rough. I can't thank you enough.

Torkjell Holm Brenna, June 2020

Contents

List of Figures

List of Tables

CHAPTER 1

Introduction

Norway is a mountainous country where snow avalanches are a common occurrence. Steep slopes and long winter seasons make the mountains ideal for ski touring and freeriding. Combined, these factors produce a significant avalanche problem, and avalanche fatalities have been recorded every year but one since 1972 (www.snoskred.no). To avoid as many fatalities as possible, efficiently forecasting avalanches is necessary, and in 2013 a national avalanche warning service was launched by the Norwegian Avalanche Centre (Engeset, 2013).

Daily avalanche bulletins are issued for the most exposed areas of Norway. They are made available to the public on varsom.no. When forecasting avalanche danger, information about the stability of the snowpack is vital. To create a complete stability assessment, physical observations are used in combination with modeled snow and weather data (Engeset, 2013). Experts analyse all available data and set an avalanche danger level for the forthcoming days.

For wet-snow, the stability can change over short time periods. As water infiltrates the snow the properties of the snowpack change, which can drastically weaken the strength of the snowpack within minutes to hours (Trautman et al., 2006). In addition, critical conditions for releasing wet-snow avalanches are difficult to assess, and periods when wet-snow avalanches can release often exists only for a short time frame. This makes it challenging for forecasting services to predict wet-snow avalanches (Techel and Pielmeier, 2009).

In recent years, studies to find adequate methods for predicting onset of wet-snow avalanche activity have been conducted. Air temperature (T_a) has commonly been used as an indicator of onset of wet-snow avalanches (McClung and Schaerer, 2006) but has been proven to produce many false alarms (Mitterer and Schweizer, 2013). In 2013, Mitterer, Techel, Fierz, and Schweizer produced a liquid water content index (LWC index) that indicates the onset of wet-snow avalanche activity reasonably well. This index uses the average volumetric liquid water content ($\theta_{w,v}$) of the snowpack to establish periods with wet-snow avalanche activity. $\theta_{w,v}$ was modeled in the 1-D energy and mass balance model SNOWPACK, updating every 3-hours, and when $\theta_{w,v}$ reaches 3% the LWC index equals 1, indicating onset of wet-snow avalanche activity.

In Norway, a less demanding model is run to produce maps of the snow cover with a 1x1 km resolution. The operative seNorge model only requires the daily

mean T_a and the daily sum of precipitation as input data to produce 1-D information about the snow water equivalent (SWE) and snow depth (SD) of a snowpack (Saloranta, 2016). From this model, $\theta_{w,v}$ can be calculated, which makes it possible to implement the LWC index in Norway. However, $\theta_{w,v}$ can change drastically within a day, thus daily updates are too infrequent. Recently, a high mountain version of the seNorge model has been developed (Saloranta, Thapa et al., 2019). In this version, the information about the snow cover can be updated every third hour, which makes it possible to update $\theta_{w,v}$ as frequently as in the SNOWPACK model.

The aim of this study is to implement the LWC index into the high mountain version of the seNorge model and try to reproduce the results that indicated the onset of wet-snow avalanche activity in the SNOWPACK model. The seNorge model will be run on data from two regions, Tyin and Tromsø, for two and four winter seasons respectively, and the model output will be compared to a registry of observed wet-snow avalanche activity in these areas.

CHAPTER 2

Theory

2.1 Avalanche Formation

Snow avalanches are generally divided into two main categories called loose-snow avalanches and slab avalanches (Lied and Kristensen, 2003). The processes around how the snowpack develops indicate which type of avalanche can occur. In general, failure of a snowpack occurs when the applied stress overcomes the strength of the snowpack. The strength can be divided into two basic components: cohesion and friction (McClung and Schaerer, 2006). Cohesion can be defined as how well the snow is held together and is directly related to the bond strength of snow grains and crystals to their neighbours. Friction is the resistance of movement between snow grains in different layers and is dependent on the texture of the snow and weight of the snow layers above. The strength of the snowpack at a given depth is determined by the sum of cohesion and friction, and generally, both of these components increase in strength downwards into the snowpack (McClung and Schaerer, 2006).

2.1.1 Loose-Snow Avalanches

Loose-snow avalanches start at a single point at or near the surface and are caused by a lack of cohesion in the snow (McClung and Schaerer, 2006). As the avalanche moves down the slope it gradually spreads out and increases in volume. At the top of the snowpack, the friction is close to zero since there are no above layers applying weight. In the right conditions, falling snow can bind together and stick to slopes with gradients up to 80°(Lied and Kristensen, 2003). As the crystals undergo metamorphism, the bonds between them will deteriorate, reducing cohesion. Since the friction is already low, this will increase the risk of loose-snow avalanches. A rapid increase in applied stress will also increase the risk of avalanches. As the cohesion and friction are low, the magnitude of the applied stress does not need to be large. Usually, loose-snow avalanches are triggered by intense precipitation. In such situations, the increase in friction due to compaction occurs too slowly to counter the increase in applied stress due to added weight (Lied and Kristensen, 2003).

2.1.2 Slab Avalanche Formation

The processes behind slab avalanches are more complicated than for loose-snow avalanches. Fundamentally, the slab avalanches initiate due to a failure associated with a weak layer at some depth in the snowpack, and all boundaries around the slab are cut out by fractures (McClung and Schaerer, 2006). Whereas loose-snow avalanches occur due to a lack of cohesion, the slab avalanches require a snow texture that is cohesive enough to form a block of snow. The processes for a slab avalanche can be explained using a three-layer model of a snowpack (figure 2.1). When a slab avalanche releases, a sudden shear fracture has taken place in the weak layer 2, causing a relatively thick and cohesive slab (layer 3) to start sliding on a sliding surface called the bed surface (layer 1 - the bed surface can also be the ground) (Lied and Kristensen, 2003). The shear fracture propagates through the weak layer, spreading both up and across the slope. As the shear fracture propagates, the attachment between the bed surface and the slab in layer 3 will be reduced. This causes a rapid tensile fracture nearly perpendicular to the bed surface at a place upslope where the snowpack is more stable, creating a wall at the top periphery of the slab called the crown fracture (McClung and Schaerer, 2006). As the crown fracture propagates across the slope, the slab will displace downslope. This causes fractures at the flanks of the slab, completely releasing the slab on all edges so that it can move freely downward. The most common trigger for natural slab avalanches is the addition of weight (McClung and Schaerer, 2006).

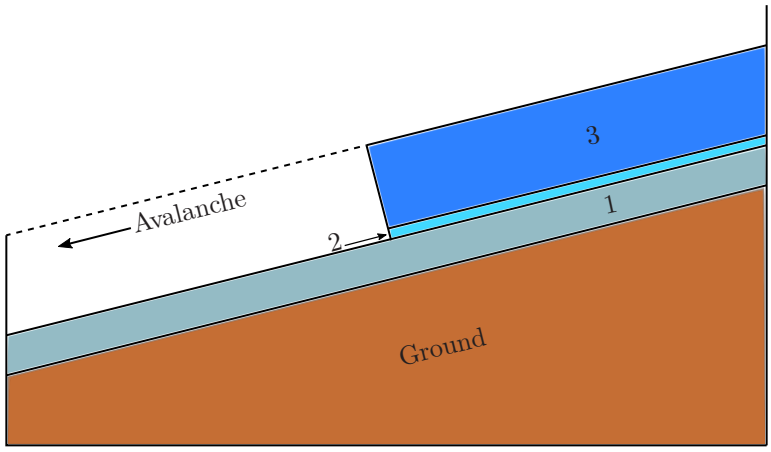

Figure 2.1: Composition of a three-layer snowpack where a slab avalanche releases. Layer 1, called the bed surface, is a dense, compact snow layer that is both cohesive and stable. The slab slides on the surface of layer 1. Layer 2 is a thin, weak layer with low hardness. Layer 3 is a relatively thick, cohesive slab. The figure is reproduced from Lied and Kristensen, 2003, p. 64.

2.1.3 Effects of Liquid Water in the Snowpack

The amount of liquid water in the snow has a large impact on the cohesion, and thus the strength of the snowpack. Water saturation varies in general from zero to approximately 20% of the pore volume (Denoth, 1980). How the water is distributed inside the pore volume can be divided into two different types of distributions: the pendular and the funicular regimes. The transition between these regimes was experimentally found to be in the saturation range of 7-15% of the pore volume (Denoth, 1980). Heat conduction is much slower in air than in water, and in the pendular regime, the air in the pore space is completely interconnected (McClung and Schaerer, 2006). Capillary pressure is dominating, and water exists mostly as thin films on snow grains. At these low levels of water saturation, the melting temperature of grain surfaces is below that of ice bonds (Armstrong and Brun, 2008). The heat will be redirected away from the bonds letting them grow and strengthen. Thus, the capillary forces can strengthen the bonding which will keep the snowpack stable. As the water content increases, the snow grains will be fully surrounded by water. In the funicular regime, the water has continuous pathways through the pore volume, and metamorphism of snow grains is caused by the heat flux through the water. A thermodynamic reversal occurs and heat flows towards the ice bonds, causing them to melt (Armstrong and Brun, 2008). As a result, saturated zones in the snow will almost be without cohesion, decreasing the strength of the snowpack substantially.

Water saturation will also affect friction. Friction between snow layers is caused by small roughness features interlocking snow layers together. Dry snow has a texture that causes high interface friction, and consequently high strength (McClung and Schaerer, 2006). When liquid water enters a snowpack, the friction is usually reduced. If water can gather between two layers in the snowpack due to an impermeable boundary, the interface becomes lubricated. The small roughness features will be covered by water, removing much of the roughness of the layer. The snow can then move nearly unimpeded over the roughness features. This will reduce the friction between the two layers substantially, decreasing the strength of the snowpack.

As water enters the snowpack, either through melting or rain, the conditions for loose-snow and slab avalanches changes. For loose-snow avalanches, the water will cause deterioration of the bonds which will reduce the cohesion. At the same time, the applied stress can increase due to loading by rain. A less cohesive snowpack can release on slopes that are less steep due to having less strength. Whereas dry loose-snow avalanches occur in inclines between 30°-60°, the wet loose-snow avalanches often release in inclines lower than 30°(McClung and Schaerer, 2006). As it moves, the avalanche pulls with it snow from below, and how deep this pull reaches determines the size of the avalanche. This is directly linked to the cohesive properties of snow with depth. As a consequence, wet loose-snow avalanches can become much larger in volume than dry avalanches. For slab avalanches, increased water saturation will trigger the avalanches through three principal mechanisms (McClung and Schaerer, 2006): added load through rain, reduced strength of the weak layer due to wet-snow metamorphism, or water lubrication of a sliding surface at an impermeable boundary in the snowpack. The last two mechanisms promote fast gliding, which causes the

tensile crack in the crown. In dry avalanches, the slab is generally released quickly after the tensile crack propagates to the top of the snowpack. For wet slab avalanches, it is also common for the slab to release several days after the crack has developed. Slab avalanches due to mechanisms associated with wet-snow have been documented to release when the air temperature was below $-10°C$ (McClung and Schaerer, 2006) (generally called glide-snow avalanches). Their wide span of response times related to a meteorological trigger makes the wet slab avalanches very unpredictable.

2.2 Avalanche Forecasting in Norway

In 2013, a national warning service was launched by the Norwegian Avalanche Center (Engeset, 2013) with the goal of reducing problems and eliminating fatalities from avalanches. Before this date, no systematic public avalanche forecasting service was available in Norway, and information about regional avalanche danger was hard to obtain. Since 2013, avalanche bulletins have been issued and made available to the public on varsom.no.

Assessing avalanche danger for a region requires data of high quality, models, and experts to analyse it. Physical observations of the snowpack are acquired by professional observers, together with recent avalanche activity and other danger signs (Engeset, 2013). This information gives an observed stability assessment of the snowpack. Data from the same area is gathered by automatic weather and snow stations. This data is used to run numerical weather prediction models and snow cover models, that provide data simulations of the current situation and a prognosis for the coming days (Engeset, 2013). A prediction of how the stability of the snowpack will develop in the near future is made from the observed and modeled data, requiring experts analysing the data and concluding a danger level. For the most exposed areas in Norway, the avalanche warning is updated every day throughout the whole winter season.

Before issuing the avalanche bulletins, several assumptions and decisions are made by experts to decide the avalanche danger level. These decisions are made from knowledge on how snowpacks and snow stability will change in different weather situations, and how this affects the avalanche probability. Judging the right avalanche danger can be hard when faced with complicated situations and with the complexity of wet-snow instability this can be especially challenging. By implementing a liquid water content index into the seNorge model, predictions on the onset of wet-snow avalanches can be continuously updated by running the model on forecasts of precipitation and T_a. Using this index removes the requirement of physical observations when forecasting wet-snow avalanche activity and can help experts in setting better avalanche danger levels when faced with situations with wet-snow instabilities.

2.3 The Liquid Water Content Index

Forecasting wet-snow avalanches is difficult due to the complex processes behind the formation of the avalanches. Water movement through the snowpack is dependent on the amount of water in the snow, with the pendular and funicular regimes. The transition between the two regimes at a saturation range of 7-15% of pore volume is equal to a volumetric liquid water content of 3-8% depending on density. Mitterer, Techel et al., 2013 used this to define a liquid water content index (LWC index) that was normalised by the starting value of the transition from pendular to funicular regime. The LWC index is given as:

$$LWC\ index = \frac{\bar{\theta}_{w,v}}{0.03} \tag{2.1}$$

where $\bar{\theta}_{w,v}$ is the modeled mean volumetric liquid water content of the entire snow cover. Conway and Raymond, 1993 points out three important periods for wet-snow instability that the index indicates: i) Snowpack stability decreases as the index increases towards 1. ii) LWC index equal to 1 indicates a completely wetted snowpack that is at maximum instability. iii) An index level above 1 for an extended time stabilises the snowpack due to ongoing wet-snow metamorphism. In theory, wet-snow avalanche activity should occur within a set time frame, n days after the LWC index passing 1.0, as shown in figure 2.2 with the red zone.

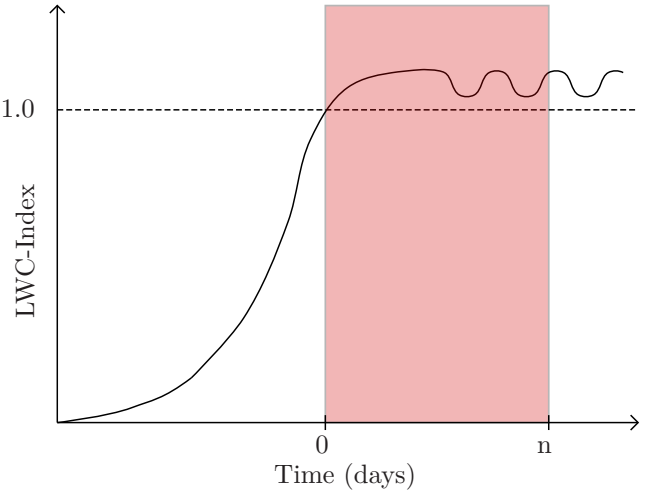

Figure 2.2: A simplified example of an LWC index for a snowpack. The stability of the snowpack decreases with the index increasing towards 1. An LWC index equal to 1.0 is a completely wetted snowpack, indicating maximum instability. In the red zone, the snowpack is still close to maximum instability, and increased wet-snow avalanche activity is expected. After n days, the snowpack has stabilised due to wet-snow metamorphism, and avalanches are no longer expected.

The LWC index was originally tested by running the index for regions in Switzerland with three different elevation bands. The mean volumetric liquid water content was modeled in the SNOWPACK model. This model requires measured mass and energy balance values and uses air temperature (T_a), relative humidity, incoming shortwave and longwave radiation, wind direction, wind speed, and snow depth (SD) as variables. The modeling of water transport is based on a simple bucket regime that depends on the simulated snow density (Mitterer, Heilig et al., 2016). An avalanche activity index was created based on the Canadian avalanche size class (McClung and Schaerer, 2006), giving weights of 0.01, 0.1, 1, 10, 100 for classes 1 to 5.

For the regional tests, the LWC index works well for days with the avalanche activity above 20. Days where high temperatures and high values of shortwave radiation caused the LWC index to increase, and little to no precipitation was recorded, gave especially good results. Two scenarios that did not record well were pointed out: i) the LWC index did not capture rain events that instantaneously caused instabilities due to the snowpack already being close to critical or loaded with new snow, nor did it capture days with low avalanche activity. ii) the LWC index did not indicate how long it takes to stabilise the snowpack through metamorphism after the index passes 1.0, meaning that there was no way to determine the end of a period with wet-snow avalanche activity (Mitterer, Techel et al., 2013). For the regional test, the LWC index did not work for the earliest wet-snow avalanches of the season, as the index indicated a dry snowpack (Mitterer, Techel et al., 2013).

The LWC index has also been tested locally on a study site above Davos for a single avalanche path (Mitterer, Heilig et al., 2016). This study showed that if there were more than one wet-snow avalanche cycle in the same path, the onset of avalanche activity occurred on different LWC index levels. For the first cycle, the avalanches match with an index level of ≥ 0.33, while the later cycle had an index level of ≥ 1. Mitterer, Heilig et al., 2016 hypothesised that the different thresholds correspond with different flow regimes for water in the snowpack. For the levels around 0.33, the water followed a preferential flow path, while matrix flow dominated the snowpack at levels around 1.0. By knowing the evolution of the snow stratigraphy and evaluating which flow will produce wet-snow instabilities, the LWC index threshold for wet-snow avalanches can be readjusted (Mitterer, Heilig et al., 2016).

A later study shows that the LWC index does not always rise to a value of 1, especially early on in the winter season (Bellaire et al., 2017). However, a sharp increase of the LWC index and high index levels is associated with increased avalanche activity. A low or decreasing LWC index is associated with periods without avalanche activity.

2.4 seNorge Model Description

Since 2004, Norway has produced snow maps with a 1x1 km resolution using the single-layer seNorge model (Saloranta, 2012; Saloranta, 2016). This model only uses T_a and precipitation as meteorological input data, simulating snow-related variables such as SD and the amount of liquid water in the snowpack. To create an LWC index in the seNorge model, these two variables are required. The version of the model that is used in this thesis is the high-mountain version described in the SnowAMP project (Saloranta, Litt et al., 2016) and applied when mapping snow conditions in Himalaya (Saloranta, Thapa et al., 2019). Instead of using daily updates as in the current operational version of the seNorge model, this version updates with a 3-hourly time step.

The seNorge model is divided into two sub-models. The snow water equivalent (SWE) sub-model handles the snowpack water balance, while the snow compaction and density sub-model change the SD (Saloranta, 2016). In the seNorge model, SWE is not affected by snow density since the SWE sub-model is kept independent from the compaction and snow density sub-model.

SWE Sub-Model

Melting of snow is applied through an extended degree-day method that has been enhanced with a solar radiation term (Hock, 2003; Pellicciotti et al., 2005). The melting rate is given as:

$$M_{eDD} = max(0, \quad b_0 T_a + c_0 SW_{net}),\ if\ T_a > T_M \tag{2.2}$$

where SW_{net} is the net shortwave radiation flux [W m^{-2}], b_0 [mm h^{-1}°C^{-1}] and c_0 [mm h^{-1} (W m^{-2})$^{-1}$] are empirical snow melt parameters, and T_M is a melt onset threshold temperature parameter (Saloranta, Thapa et al., 2019). The $SW_{net} = (1 - \alpha_s) \cdot SW_{in}$, where the formulation by Allen et al., 2006 of incoming solar radiation (SW_{in}) is used. SW_{in} is calculated for an inclined grid cell with a defined slope and aspect, which takes into account the attenuation in the atmosphere as well as diffuse solar radiation. The snow surface albedo (α_s) is calculated by using the model from Tarboton, Luce et al., 1996.

The snowpack can refreeze if the T_a is below 0°C and no melt occurs (Saloranta, Thapa et al., 2019). The refreezing of liquid water within the snowpack was updated in the SnowAMP project and is based on a modified Stefan's law analytical model which was originally developed for sea ice freezing (Leppäranta, 1993). The refreezing of liquid water is modeled as a "refreezing front" which moves from the top of the snowpack and downwards. This takes into account that liquid water refreezes more easily in top layers of the snowpack than further down due to snow being a good thermal insulator. The depth of the refreezing front z_{rf} [m] is formulated as:

$$z_{rf}^{t} = \sqrt{\left(z_{rf}^{t-1}\right)^2 + \frac{2\kappa_s}{\rho_{lw} L} \cdot (-T_a)\, \Delta t},\ if\ T_a < 0°C \tag{2.3}$$

where κ_s is the thermal conductivity of snow [W m^{-1} K^{-1}], L is the latent heat of fusion [J kg^{-1}], ρ_{lw} is the partial density of the liquid water residing

in the snowpack [kg m^3], Δt is the time step [s], and superscripts t and $t-1$ denote the current and previous time steps, respectively (Saloranta, Thapa et al., 2019).

κ_s is parameterised as a function of snow density (ρ_s) (Yen, 1981) and is applied in the model as $\kappa_s = 2.22362 \cdot (\rho_s)^{1.885}$, where ρ_s is the snow density [kg L^{-1}]. Below the "refreezing front", a homogeneous distribution of the liquid water is assumed. This causes ρ_{lw} to be equal to liquid water content (W_L) divided by the SD. Since the SWE sub-model is kept independent from the density sub-model, a constant value for ρ_s is set and $\rho_{lw} = \rho_s \cdot W_L / SWE$. The "refreezing front" is moved back to the top of the snowpack ($z_{rf} = 0$) whenever a new input of liquid water is added to the snowpack, either as snowmelt or rain. This indicates that liquid water is present throughout the whole snowpack (Saloranta, Litt et al., 2016).

The snowpack can only contain liquid water (SWE_{liquid}) up to a fraction r_{max} of the ice content (SWE_{ice}). Melt-water and precipitation falling as rain go into the snowpack until this limit met. After that, the excess is set as runoff. This means that melting of the snowpack does not impact the SWE_{total} immediately but converts SWE_{ice} to SWE_{liquid} first. As a result, the capacity for liquid water in the snowpack will be reduced. For refreezing this is reversed: the water is transferred back from liquid to solid phase without changing the SWE. This, in turn, will increase the ice fraction and the amount of liquid water the snowpack can hold. Consequently, the runoff will be reduced and the snow density of the snowpack will increase (Saloranta, Litt et al., 2016).

Snow Compaction and Density Sub-Model

In the snow compaction and density sub-model, the SD [mm] is calculated with changes occurring due to snowmelt, new snowfall, and viscous compaction (Saloranta, 2016). The model starts by decreasing SD due to snowmelt and/or increasing due to new snowfall. The density of newly fallen snow (ρ_{ns}) is calculated as a function of T_a as in Bras, 1990:

$$\rho_{ns} = \rho_{ns\,min} + \left(\frac{max[0,\ 1.8 \cdot T_a + 32]}{100} \right)^2 \tag{2.4}$$

where $\rho_{ns\,min}$ is the minimum density of new snow (Saloranta, 2016).

To calculate the decrease of SD due to gradual compaction (ΔSD_{comp}), the common assumption that snow behaves as a viscous medium is used (Yen, 1981):

$$\Delta SD_{comp} = -\frac{m_s}{\eta} SD \cdot \Delta t \tag{2.5}$$

where m_s is the force [N/m^2] due to the weight of the snowpack over the layer which compaction is calculated, η is the viscosity of the snow [Ns/m^2], and Δt is the step [s]. Since the seNorge model has a single layer snowpack, $m_s = 0.5 \cdot g \cdot SWE$, where g is the gravitational acceleration near Earth's surface (9.81 m/s^2) (Saloranta, 2016). η follows the formulation as in the Crocus snow model (Vionnet et al., 2012):

$$\eta = \frac{1}{1 + 60\frac{W_L}{SD}} \cdot \eta_0 \cdot exp(-C_5 T_{snow} + C_6 \rho_s) \tag{2.6}$$

where W_L [mm] is the liquid water content, T_{snow} [°C] is the the temperature of the snowpack, and ρ_s is the density of the snowpack. T_{snow} is approximated from T_a and is defined as $min(0.5 \cdot T_a,\ 0)$. η_0, C_5 and C_6 are constant model parameters (Saloranta, 2016).

The LWC index is calculated for each time step using one variable from each sub-model. As the model considers a single layer bulk snowpack, the average liquid water content ($\bar{\theta}_{w,v}$) can be calculated from SD and liquid water content. This gives the LWC index for the seNorge model as:

$$LWC\ index = \frac{\frac{SWE_{liquid}}{SD}}{0.03} \tag{2.7}$$

CHAPTER 3

Method

3.1 Study Sites

To test how well the LWC index works with the seNorge model a register of wet-snow avalanches is required. This data was provided by NVE (The Norwegian Water Resources and Energy Directorate) for two regions, Tyin and Tromsø, for two and four winter seasons, respectively.

3.1.1 Tyin

Tyin is a lake in south-western Jotunheimen. The area around the lake is exposed to many avalanches. Because of a county road (FV.53) that goes through this area, there is active surveillance for the most exposed parts. Avalanches are registered by qualified observers, who upload their reports to regobs.no. The avalanche activity for the two winter seasons from 2016 to 2018 was provided by NVE together with the regobs registry. For this period, there were 277 avalanches registered, with over 200 of them being triggered manually by explosives. Of 74 naturally released avalanches, only 15 were defined as wet-snow avalanches. The locations of the avalanches were given as GPS coordinates for pictures taken of the avalanches. A map of the area marked with the given GPS coordinates is shown in figure 3.3. The avalanches are spread out in a small area, with around 5 km between the avalanches furthest apart, and two of the pictures used for locating the avalanches are shown in figures 3.1 and 3.2.

By looking at the pictures, together with maps, the avalanche locations were set. Since the quality of the pictures varied, some avalanches were harder to precisely pinpoint than others. Thus, there is a possibility that the wrong 1x1 grid cell data (see Weather Data section) have been used to run the seNorge model. However, since the pictures were taken close to the avalanches the GPS locations were either in the right 1x1 km grid cells or neighbouring the right grid cells. Neighbouring grid cells in the area around Tyin are roughly at the same altitude and have, as a consequence, close to the same temperature and precipitation data. Choosing the neighbouring 1x1 grid cell is therefore thought to have a negligible effect on the LWC-index.

Figure 3.1: Picture of wet-snow avalanches that released by lake Tyin on 15/04/2018. Picture was taken from regobs.no.

Figure 3.2: Picture of wet-snow avalanches that released by lake Tyin on 15/04/2018. Picture was taken from regobs.no.

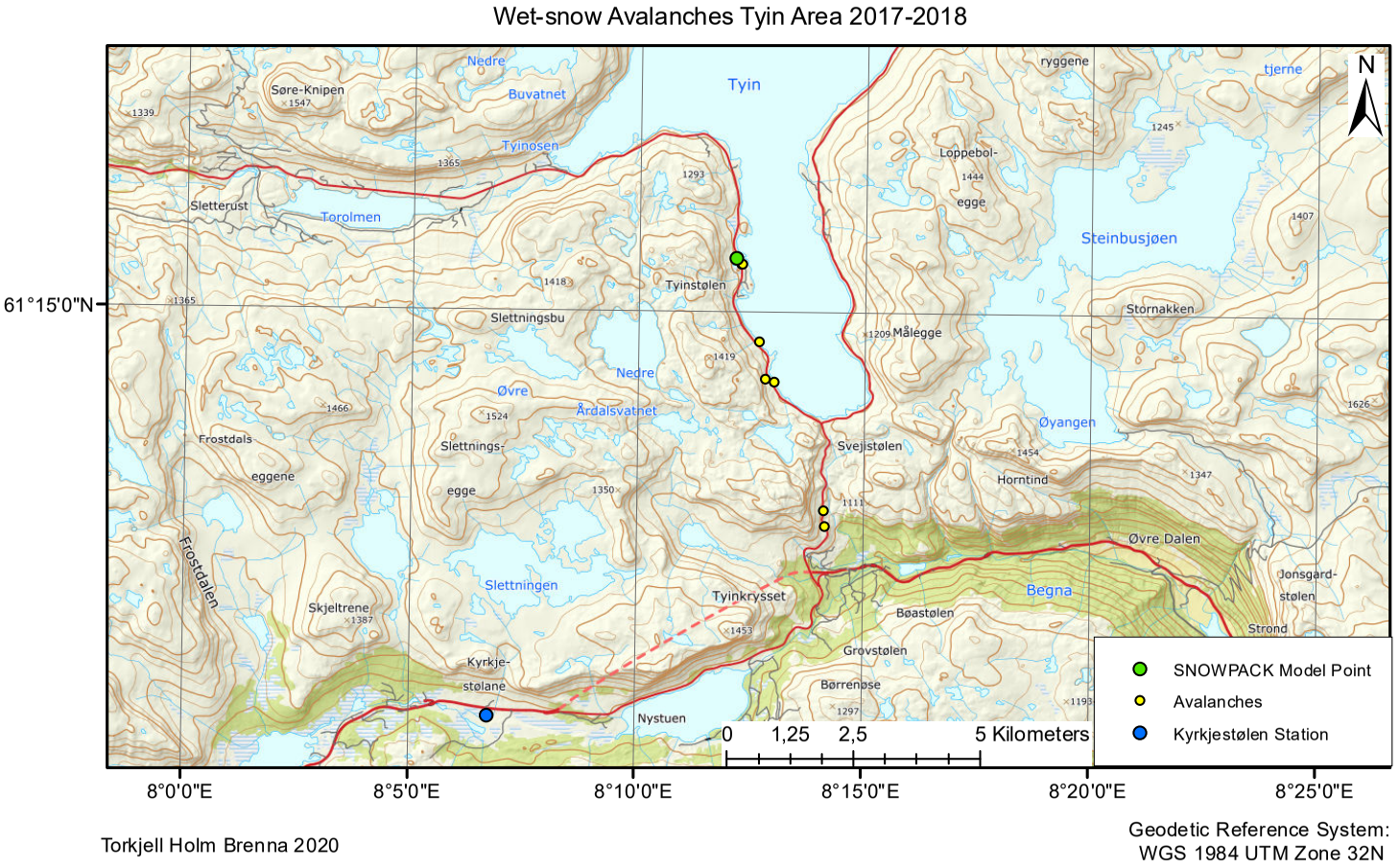

Figure 3.3: Avalanche area by lake Tyin. The yellow points are the GPS locations of the pictures taken of the wet-snow avalanches nearby, thus it is not the exact locations of the avalanches. Point data from the SNOWPACK model is given at the location of the green mark. The blue dot is the weather station at Kyrkjestølen, which both models have been run on. The map has been created using a WMS from kartverket.no

3.1.2 Tromsø

In the area around Tromsø, there have been registered 219 wet-snow avalanches during the winter season from 2015 to 2019 (with zero observations in 2016). The dataset containing dates and point coordinates of all the avalanches was collected by NORCE and provided by NVE. The avalanches have been mapped using SAR satellite images, and the avalanche locations have been validated either by measurement from people on-site or estimated from distance in a helicopter. Of the 219 avalanches, 187 have been used in the testing of the LWC index. The locations of these are shown in figure 3.4. Locations of the avalanches were not certain, as only a point coordinate was given for every avalanche. There was no information about whether the points were release points or at the end of the runout. Many of the avalanches were close to a boundary between two 1x1 grids on Xgeo, and the differences in elevation and temperatures from one grid cell to the next could be large. All avalanches in the Tromsø region were therefore processed on both the lower and upper grid cells near the avalanches to observe the effect this had on the LWC index compared to the avalanches.

3.1.3 Weather Data

T_a and precipitation is required to calculate the LWC index for the seNorge model. This data is available from xgeo.no, a website containing maps of temporal and spatial data for Norway. The data are either real-time point observations from weather stations, or interpolated weather observations and numerical predictions (Barfod et al., 2013). Norway is divided into grid cells of 1x1 km for interpolation purposes. For each grid cell the T_a and precipitation is interpolated, thus the LWC index can be calculated for every grid cell for the entirety of Norway. One value is given for the elevation for the entire grid cell. This elevation is measured from the middle of a 20-m resolution digital elevation model (DEM). To resample the DEM from 20-m to 1-km, a nearest neighbour interpolation was used (Tuomo Saloranta, personal communication, June 9, 2020). The advantage of setting the elevation this way is to properly differentiate between the floor of a valley and the mountaintop. However, this causes the elevation of the slopes where avalanches occurs to often vary significantly from the elevation grid cell.

For the Tyin area, the seNorge model has been run on station data from Kyrkjestølen weather station (figure 3.3) and grid data around the avalanche points. The station data is used to evaluate how the seNorge and SNOWPACK model compare to observed data by comparing the modeled to the observed SWE and snow depth. Observed solid precipitation measurements can be undervalued as a consequence of wind-caused undercatch. Up to 80% of actual solid precipitation at $-2°C$ or below can be missed by measuring equipment as a result of high wind speeds (Wolff et al., 2015). Liquid precipitation measurement does not have the same margin of error. To evaluate the effect this would have on the LWC index for the seNorge model, several different factors up to a factor of 2.40 have been added to the solid precipitation data from Kyrkjestølen station. Since wind speed is not taken into account, this is a very simple approximation with a constant factor added to the solid precipitation.

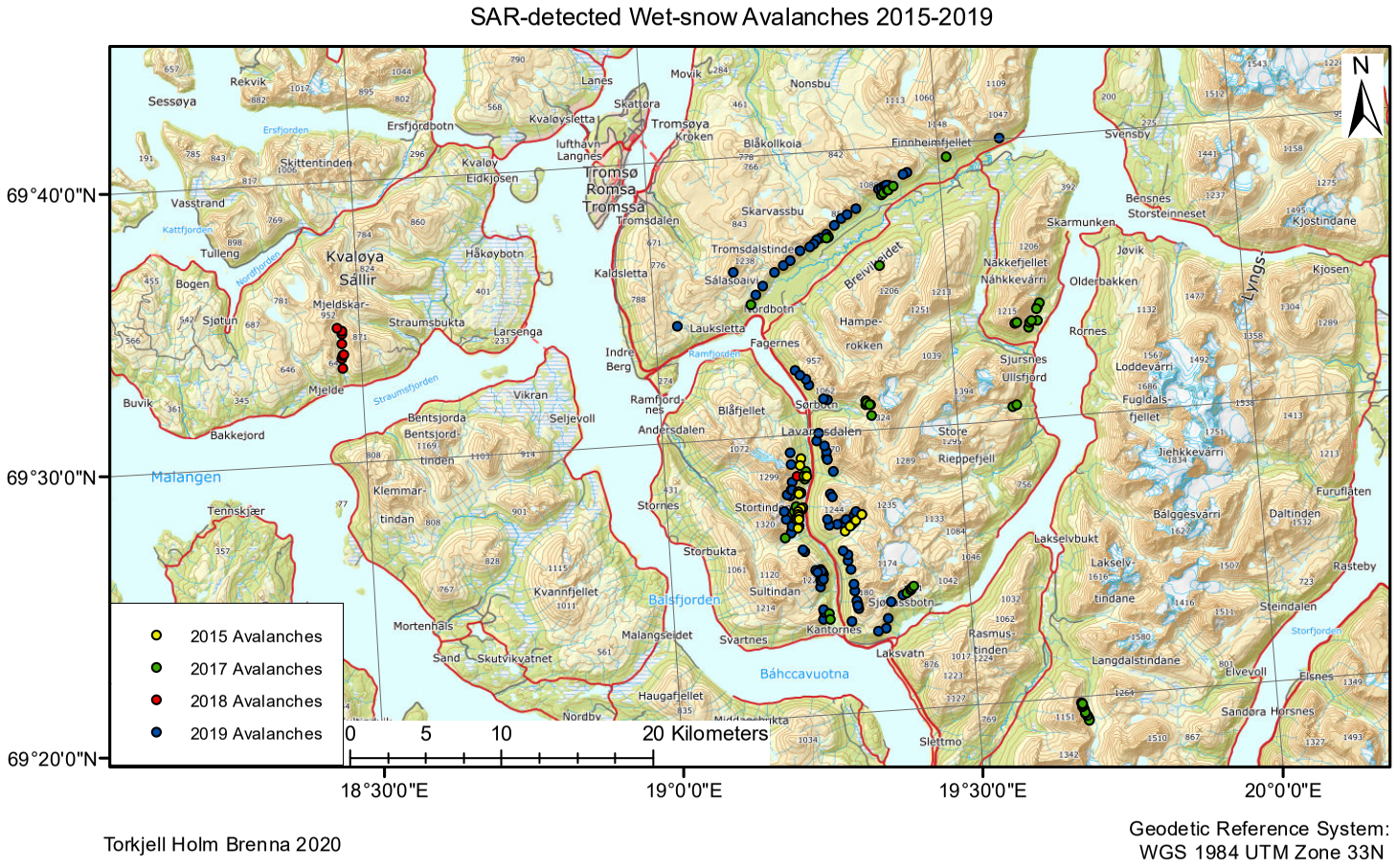

Figure 3.4: Wet-snow avalanches detected with SAR satellites in the region south of Tromsø. 95 avalanches in 2019 (blue marks), 10 avalanches in 2018 (red marks), 60 avalanches in 2017 (green marks), and 22 avalanches in 2015 (yellow marks). The map has been created using a WMS from kartverket.no

3.2 Models

3.2.1 seNorge Model

The model scripts for the high-mountain version (v.2) of the seNorge model are coded in the open-access software R. All scripts were run on a local PC, only requiring a three-hourly dataset of T_A and precipitation. This data was downloaded from xgeo.no in 1x1 km grid cells.

To calculate SW_{net} in equation 2.2, geographical information about the grid cell was used together with the weather dataset: latitude, elevation, aspect of slope, and slope angle. The aspect of the slopes was estimated from map data on xgeo.no. The precise location of the avalanches was not known in either region. This makes it difficult to find the correct slope gradients. Due to time constraints, all slope angles are set to 38°, which was the slope angle of the virtual slopes in the regional analysis in SNOWPACK (Mitterer, Techel et al., 2013). This causes the SW_{net} to only change with elevation, aspect, and time of year.

The model parameters to run the model have been replicated from the high-mountain application of the seNorge Model and the SnowAMP project (Saloranta, Litt et al., 2016; Saloranta, Thapa et al., 2019) and are shown in Table 3.1. Here, the parameters relating to snowmelt have been changed from the operative version of seNorge. In this 3-h version of the model, the melt parameters are optimised against observations from station data in Himalaya (Saloranta, Thapa et al., 2019). Clear-sky radiation was assumed in the algorithm when the new melt parameters were estimated. Consequently, the cloud fraction is set to 0 in the SW_{in} equation (Allen et al., 2006). In general, the SW_{net} will be at the lowest in mid-winter and increase in value towards the spring. This will cause melting in mid-winter to only occur with T_a above 0°C, while the melting can occur closer to the T_a threshold for the onset of melting in spring. Some of the parameters have different values depending on whether the grid-cell is above or below the treeline. In the area around Tromsø, this was approximated to 550 m.a.s.l (Bryn and Potthoff, 2018), while all grid cells in the Tyin area were set above the tree line with avalanches in grid cells above 1100 m.a.s.l.

Table 3.1: The main SeNorge model parameters as replicated from the high-mountain application (v.2) of the seNorge model.

Parameter	**Description**	**Value**	**Value above treeline**	**Unit**
r_{max}	Maximum allowed liquid/ice weight fraction of liquid water in snowpack	0.11	NA	[-]
T_{thr}	Threshold air temperature for solid/liquid precipitation	0.5	NA	[°C]
T_M	Trehshold air temperature for snowmelt onset	-3	NA	[°C]
b_0	Melt rate parameter	0.33	0.33	[mm h^{-1} $°C^{-1}$]
c_0	Melt rate parameter	0.0086	0.0086	[mm h^{-1} $(Wm^{-2})^{-1}$]
ρ_{srf}	snow density used in refreezing algorithm	0.270	NA	[kg/L]
$fSCA$	Spatial snow distribution parameter	0.25	0.50	[-]
ρ_{nsmin}	Minimum density of new snow	0.050	0.100	[L/kg]
η_0	Initial snow viscosity at 0°C and 0 kg/L	7.622	NA	[MN s m^{-2}]
C5	Coefficient for temperature effect on viscosity	0.1	NA	[$°C^{-1}$]
C6	Coefficient for density effect on viscosity	24.3	NA	[L kg^{-1}]

3.2.2 SNOWPACK Model

The SNOWPACK model has been run for two locations at Tyin. The locations of these points are shown in figure 3.3, with one point being directly on Kyrkjestølen weather station. Wyssen Avalanche Control Centre ran the SNOWPACK model and provided a dataset with the model's output. This dataset consisted of modeled snow depth, average liquid water content, and the LWC index from 2016 to 2020. No information about the input to the model was given, other than that the precipitation data was from Kyrkjestølen weather station with a prescribed vertical gradient with altitude to the given point.

With only information about three output variables given, only a comparison between snow depth and LWC index could be done between the SNOWPACK model and the seNorge model. Specifying whether model differences come from the different model algorithms or different inputs is unachievable without more information. However, since both models have been run on Kyrkjestølen weather station, it is possible to determine how well they perform up against the observed station data.

CHAPTER 4

Results

4.1 Tyin

4.1.1 Modeled Data Compared to Measurements on Kyrkjestølen Weather Station

The observed and modeled snow depths at Kyrkjestølen station from 2016 to 2018 are shown in figure 4.1. The seNorge model without a solid precipitation factor and the SNOWPACK model have values below the observed snow depth most of the time.

For the 16-17 winter season, the observed snow depth has rapid increases in early November and late December, with both modeled snow depths only having small increases in the same periods. In late December the observed snow depth increases by 70 cm in five days, whereas the modeled snow depths increase by approximately 10 cm in the same time frame. In this interval, the registered precipitation is 12 mm. From March and towards the end of the season, both the original seNorge model and the SNOWPACK model follow the same trend as the station data but at a lower snow depth. The modeled snow depth for the seNorge model is continuously between 30-40 cm lower than the observed station data, with the SNOWPACK model being 10-15 cm below that level. The last day of snow is measured on May 24. This is 13 and 11 days after the snow is gone in the SNOWPACK model and the original seNorge model output.

In 2017-2018, both models heavily underestimated the snow depth again, but this time the original seNorge model snow depth is below the SNOWPACK output. The buildup of snow until mid-December is reasonable for both models, staying within 10-15 cm of the observed snow depth. From the middle of December until the season's maximum, the snow depth at the station increases with approximately 100 cm. At the same time, the snow depth for the SNOWPACK model increases with 60 cm and the seNorge model only increases by 30 cm. The last day of snow is measured on May 18. This is 7 days before the snow is completely melted in the SNOWPACK model on May 25. For the original seNorge model, this day occurs on May 5.

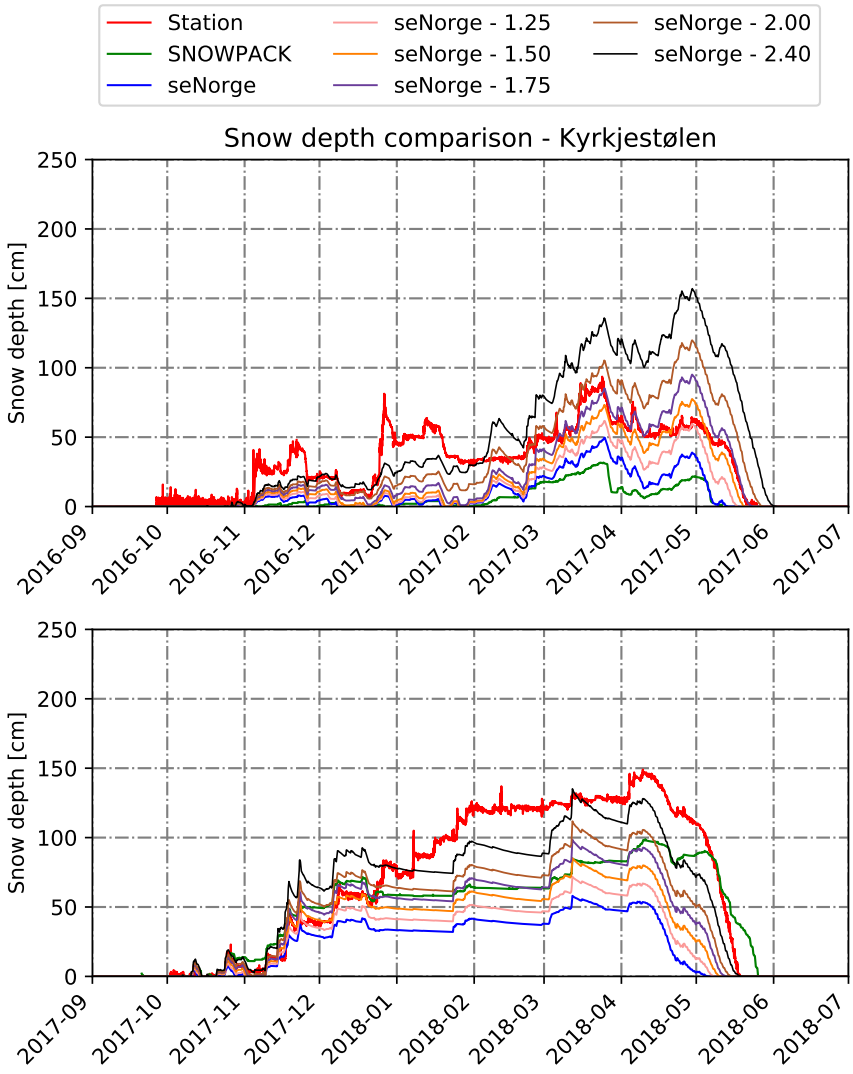

Figure 4.1: Snow depth measured in cm at Kyrkjestølen station from 2016 to 2018. The seNorge and SNOWPACK model ran on the observed precipitation and temperature data at the station to model snow depth. For the seNorge model, the solid precipitation data have been multiplied, giving six different outputs.

The SWE is also measured on Kyrkjestølen. In figure 4.2, the observed SWE and the modeled SWE from the seNorge model are shown. For the 16-17 winter season, the observed data is incomplete, as the station only has records from mid-February. From the middle of March, the original seNorge model's SWE is around 200 mm less than the registered station data, a difference that is stable all the way to the end of the season.

The 17-18 winter season has an SWE that shows the same as the snow depth. The buildup of snow for the model is within a reasonable difference from the station at the beginning of the season. The model then flattens out from mid-December while the station levels continue to rise. From that point and onward to the peak, the SWE for the seNorge model increase by approximately 80 mm. The station data increases with over 400 mm in the same time frame. Looking at the registered precipitation at the station, only 80 mm are recorded from mid-December to mid-April.

For the seNorge model, the solid precipitation data have been multiplied with six different factors (figure 4.1 and 4.2). This makes the model output come closer to that observed on the station. In 2016-2017, the model running on the 1.50 multiplier have a snow depth that differs within 5-20 cm of the station data from late February until the end of the season. With a 1.75 multiplier the, modeled snow depth stays around the same level as the station data from late March and until the end of the season, but the increase in late April differs with over 35 cm from the station data. For the SWE, the 1.75 and 2.00 multipliers have outputs coming closest to the observed data. For the modeled snow depth and SWE that is within a reasonable distance from the observed station data, the melts rates are approximately the same as the observed melt rates.

For the 17-18 season, a factor of 2.40 is added to the solid precipitation. This causes the modeled snow depths and SWE to be much closer to the station data but still some levels below. This output has a snow cover that lasts nearly as long as the station data and indicates a melt rate that is near that observed on the station.

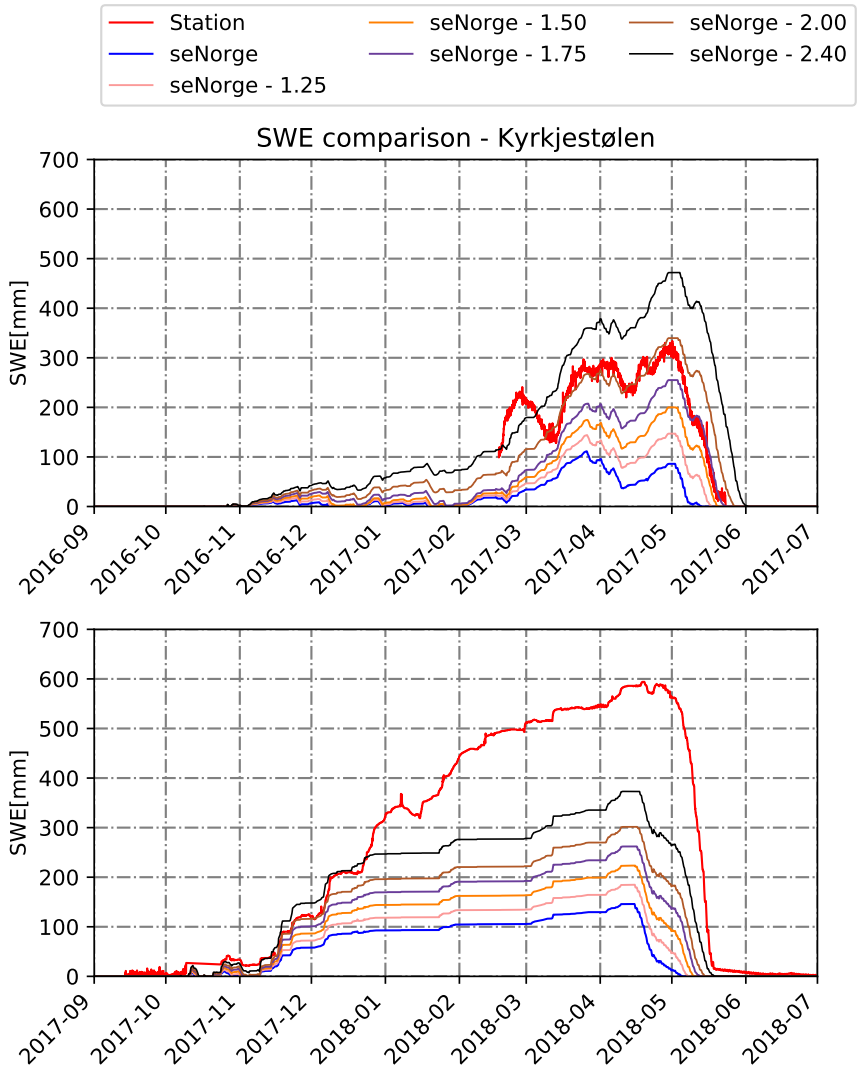

Figure 4.2: SWE measured in mm at Kyrkjestølen station from 2016 to 2018. The seNorge model ran on six different factors of the observed solid precipitation at the station to model the SWE. For the 16-17 winter season, the observed data is incomplete and did not start until February 17.

In figure 4.3, 4.5 and 4.4, the modeled LWC indexes for the SNOWPACK and the seNorge model is shown. With how much the modeled snow depth and SWE vary from the observed station data, the LWC index has been included for all factors of solid precipitation. The three periods shown in the figures are periods where wet-snow avalanches occurred.

For the seNorge model, the modeled LWC indexes do not show large differences between the original solid precipitation and the added multiplication factors. The first time the LWC indexes pass maximum instability in spring 2018 is around April 15 (figure 4.4). By adding a factor of 2.40 to the solid precipitation the LWC index rises at the same time but passes 1.0 approximately two days after the original index. Diurnal fluctuations to the index occur at the same time, but with larger amplitude, the lower the multiplier used. The LWC indexes end at different times due to the snowpack completely melting at different times.

In spring 2017 (figure 4.3), the initial rise of the LWC indexes occurs on 01/04. As in 2018, the LWC index with a 2.40 factor added to the solid precipitation peaks under two days after the original seNorge model index. After the initial rise, the snowpack gradually refreezes again, shown in the LWC index as a decreasing curve. The modeled LWC indexes that have a larger snowpack (higher multiplication factor used) decreases slower than smaller snowpacks. This can be seen between 15/04 and 01/05. Here the modeled output using the original precipitation data decreases to 0, while the LWC index for the 2.40 multiplier is at 0.45 on the same day.

The LWC indexes in December 2017 and January 2018 (figure 4.5) rises and decreases at the same time, but with small differences in the rates. The higher the multiplier on solid precipitation, the lower the index initially rises on 20/12/2017, but with a higher peak on 23/12/2017. The time to refreeze the whole snowpack takes longer with larger multipliers for solid precipitation used, as the snowpack becomes thicker.

The modeled LWC index for the SNOWPACK model has varying results compared to the seNorge model. In December 2017, the LWC index for the original seNorge data and SNOWPACK data is close to equal in the initial rise, but the index for the SNOWPACK model does not have a secondary peak on 23/12 (figure 4.5). Throughout spring 2017 both models have an index that is fluctuating. For the SNOWPACK model, this fluctuation is more rapid, and the index varies between 0 and above 1.5 several times in a short time frame (figure 4.3). In 2018, the LWC index for the SNOWPACK model is completely different from the seNorge model index. The initial increase to the LWC index occurs earlier for the seNorge model than for the SNOWPACK model. While the index for the seNorge model passes 1.0 and starts with diurnal variations, the SNOWPACK index increases up to 0.8 before declining back to 0. When the LWC index first passes maximum instability, it is three weeks after the seNorge model passing the same threshold.

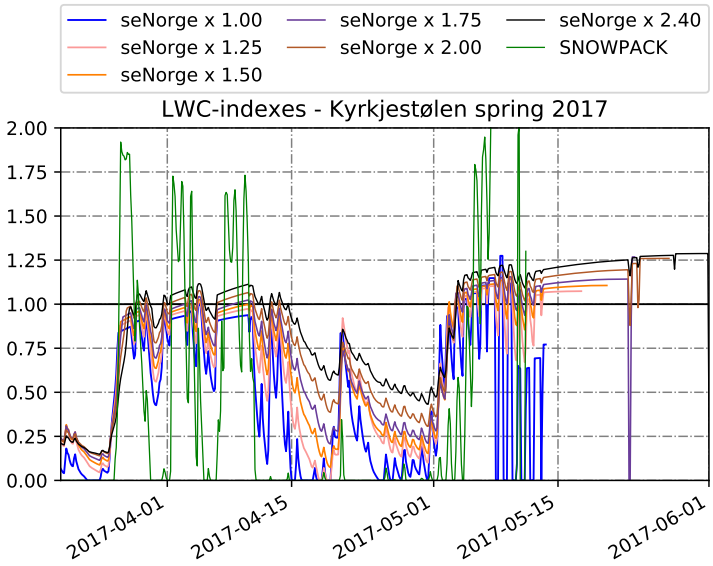

Figure 4.3: LWC indexes modeled with weather data from Kyrkjestølen station for spring 2017. The seNorge model has been run with six different solid precipitation multipliers, creating six different outputs.

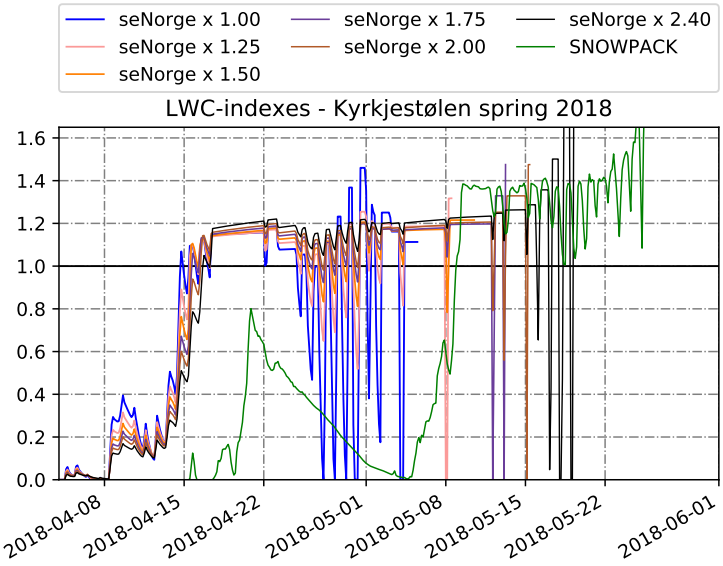

Figure 4.4: LWC indexes modeled with weather data from Kyrkjestølen station for spring 2018. The seNorge model has been run with six different solid precipitation multipliers, creating six different outputs.

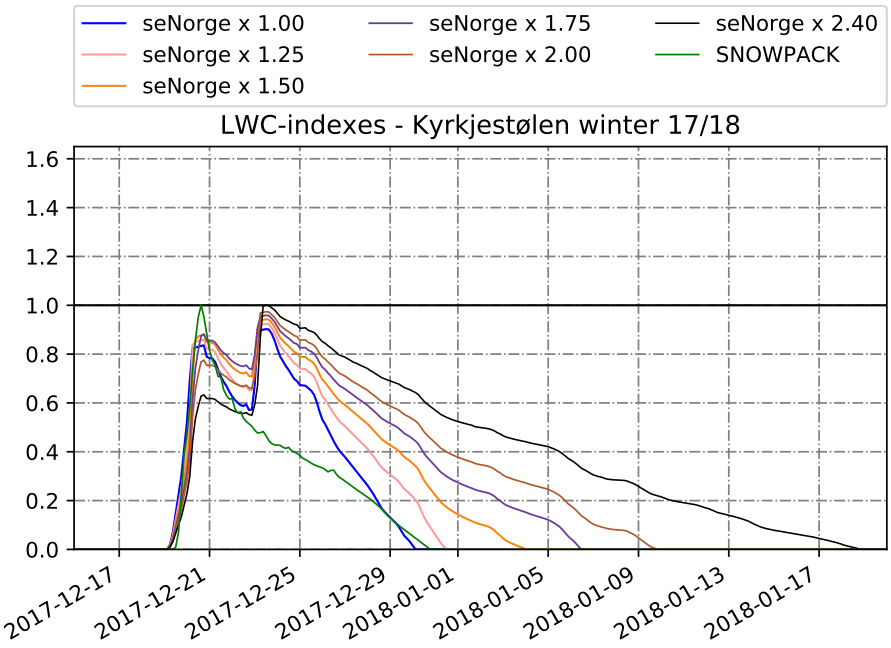

Figure 4.5: LWC indexes modeled with weather data from Kyrkjestølen station for December 2017 and January 2018. The seNorge model has been run with six different solid precipitation multipliers, creating six different outputs.

4.1.2 LWC-index Compared to Avalanche Activity at Tyin

The 15 wet-snow avalanches at Tyin are all on east-facing slopes, spread out over four different grid cells. The grid cells farthest away from each other are approximately 5 km away in distance, with the other grid cells in between these two. Table 4.1 shows how the avalanches are spread out over different dates, and the elevation of the grid cells used for precipitation and temperature data. The LWC indexes have been created from this data by running the seNorge model without a solid precipitation factor. The LWC index for the SNOWPACK model has an elevation of 1098 m.a.s.l. and is located on a point close to the avalanches furthest north (20/12/2017 and 19/04/2018 avalanches).

Date	Avalanche Count	Elevation of Xgeo Grid Cell
18.05.2017	3	1251 m.a.s.l.
20.12.2017	2	1208 m.a.s.l.
	2	1084 m.a.s.l.
15.04.2018	3	1235 m.a.s.l.
16.04.2018	1	1235 m.a.s.l.
19.04.2018	1	1208 m.a.s.l.
20.04.2018	3	1251 m.a.s.l.

Table 4.1: Date of wet-snow avalanches at Tyin and their respective Xgeo grid cell elevation.

In figure 4.6, the avalanches in May 2017 and the LWC indexes are shown. The index for both the SNOWPACK and the seNorge model starts rising on 01/05. For the SNOWPACK model, the index passes 1.0 two days later. However, there are diurnal fluctuations causing the LWC index to vary by values of over 0.75 for days and nights. For the SNOWPACK model, the snow cover is completely melted by 06/05, with some sudden daily spikes after this date due to new snowfall.

The LWC index for the seNorge model follows the same trend in rising and falling as the SNOWPACK model, but the fluctuations are much smaller. The index rises on 01/05 and passes maximum instability on 05/05, 13 days before the observed avalanches. The fluctuations of the LWC index coincide with the large diurnal fluctuations of the observed temperatures. Daily temperatures reach values above 5°C, with nightly temperatures below −5°C. After 05/05 the LWC index flattens out, with a short refreezing period due to four days with colder temperatures and small amounts of precipitation. From 13/05, the temperatures are above the threshold for liquid precipitation, both day and night. On the day of the avalanches over 18 mm of precipitation falling as rain is registered throughout the day.

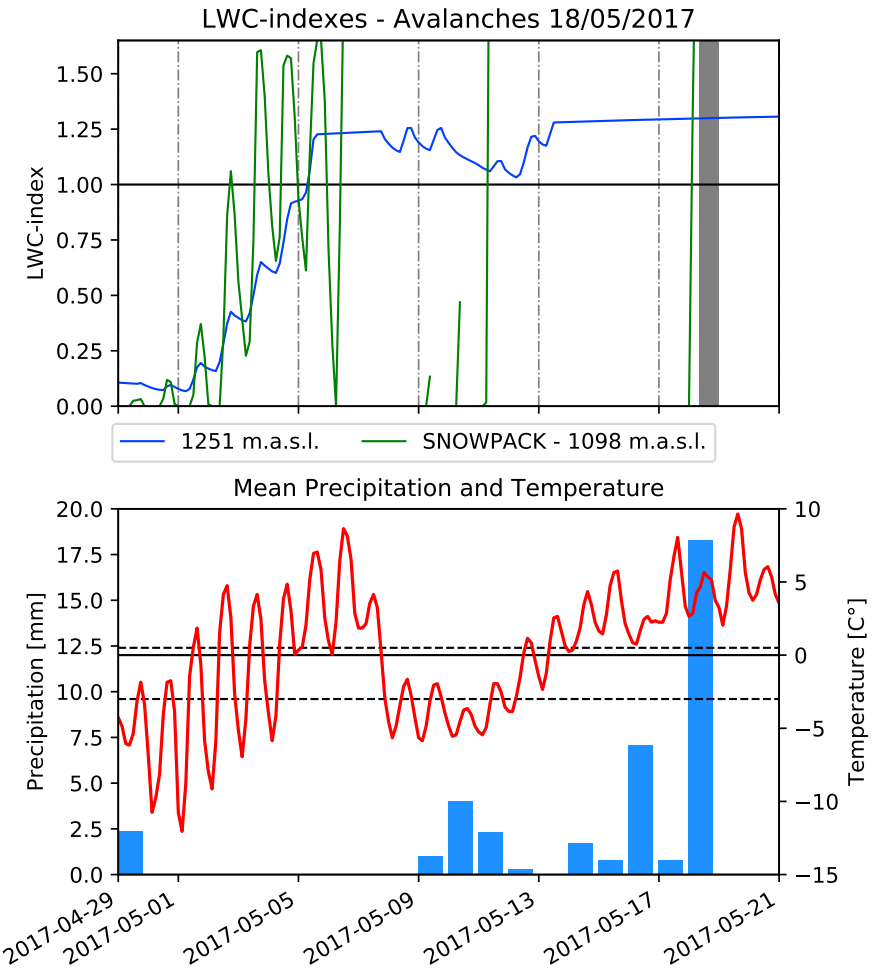

Figure 4.6: 1) LWC indexes for avalanches on 18/05/2017. The SNOWPACK model is run on point data with an elevation of 1098 m.a.s.l. and approximately 2km away from the avalanche. The seNorge model uses the Xgeo grid (elevation 1251 m.a.s.l.) data where the avalanches are located within the grid. The possible time of onset for the avalanches is shown as a grey bar.
2) The precipitation and temperature data used to run the seNorge model. Daily summed precipitation is shown as blue bars, while temperature data is plotted every 3-hour in red lines. The two dotted black lines indicate the threshold air temperature for liquid or solid precipitation and possible temperature onset of melting in the model, on 0.5°C and −3°C respectively.

The avalanches in April 2018 occurs at four different days, within three different grid cells. The distance between the grid cell farthest north and the one farthest south is approximately 5 km, and the elevation only varies with around 40 meters. The modeled LWC indexes for these avalanches are shown in figure 4.7, with the mean precipitation and temperature of the three grid cells used to run the seNorge model.

The three LWC indexes for the seNorge model are close to identical, having a maximum difference of 0.05 at a few places. These indexes start to rapidly increase on 14/04/2018, with temperatures increasing up to 5°C during the day. The LWC index passes maximum instability the day after (15/04) and flattens out. Some diurnal fluctuations occur after this point, due to negative temperatures during the night and positive temperatures during the day. The avalanches releases five days, four days, and before and on the same day the LWC index passes maximum instability. On the dates of the avalanches, no rain is recorded for the most part, with around 1 mm of precipitation on 20/04.

For the SNOWPACK model, the LWC index does not start to increase before the evening on 19/04, and peaks on a value of 0.7 one day later. Thus the LWC index increases on two of the dates where avalanches occur without passing maximum instability. The mean temperature for the seNorge model is continuously above the threshold for liquid precipitation when the LWC index for the SNOWPACK model increases, with around 1 mm of precipitation recorded.

The avalanches on 20/12/2017 are spread out over two different grid cells, which is about 2 km apart. The modeled LWC indexes can be seen in figure 4.8 with the temperature and mean precipitation for the two grid cells used to run the seNorge model. All three indexes start to rise on the evening of 19/12, peaking on the day of the avalanches. This coincides with temperature rapidly increasing from below −5°C to above 2.5 °C. Around 5 mm of precipitation is registered when the indexes increase, modeled as rain due to the temperature being above the threshold for liquid precipitation. None of the LWC indexes reaches maximum instability on 20/12, with the lowest elevation grid cell peaking on an index level of 0.9 and the SNOWPACK model only reaching an index level of 0.6. On the same day, the indexes start to decrease again due to temperatures dropping below −2°C.

The LWC indexes for the SNOWPACK model and the lowest elevation seNorge model start to increase and pass maximum instability on 23/12, before instantly starting to decrease again. On this date, nearly 10 mm of precipitation is recorded and temperatures rapidly increase from around −3°C towards positive temperatures. For the grid cell with an elevation of 1084 m.a.s.l., the temperatures pass the threshold temperature for liquid precipitation, meaning that the 10 mm of precipitation fall as rain. For the grid cell with a higher elevation, the temperatures are just below this threshold, causing all the precipitation to fall as snow.

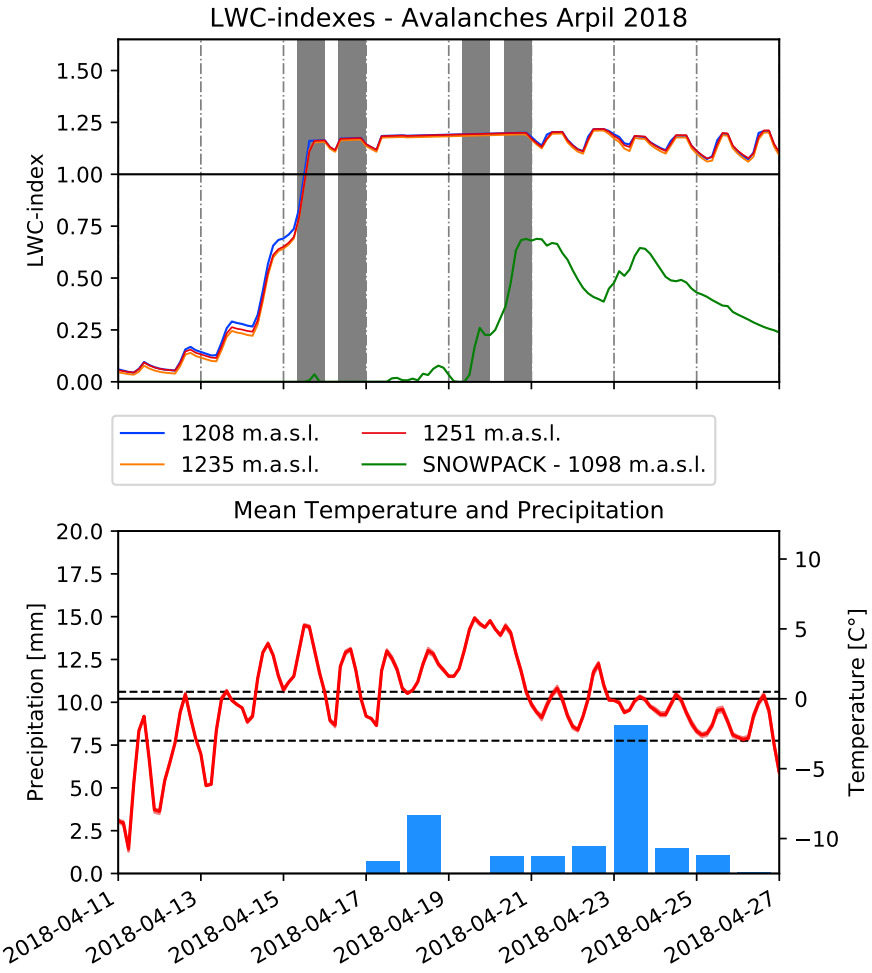

Figure 4.7: 1) LWC indexes for avalanches April 2018. The SNOWPACK model is run on point data with an elevation of 1098 m.a.s.l. which is approximately at the avalanches furthest north. The seNorge model uses the Xgeo grid (elevation 1208, 1235, and 1251 m.a.s.l.) data where the avalanches are located within the grid. The possible time of onset for the avalanches is shown as a grey bar.
2) The mean precipitation and temperature data from the three grid cells used to run the seNorge model. Daily summed precipitation is shown as blue bars, while temperature data is plotted every 3-hour in red lines. The two dotted black lines indicate the threshold air temperature for liquid or solid precipitation and possible temperature onset of melting in the model, on 0.5°C and −3°C respectively.

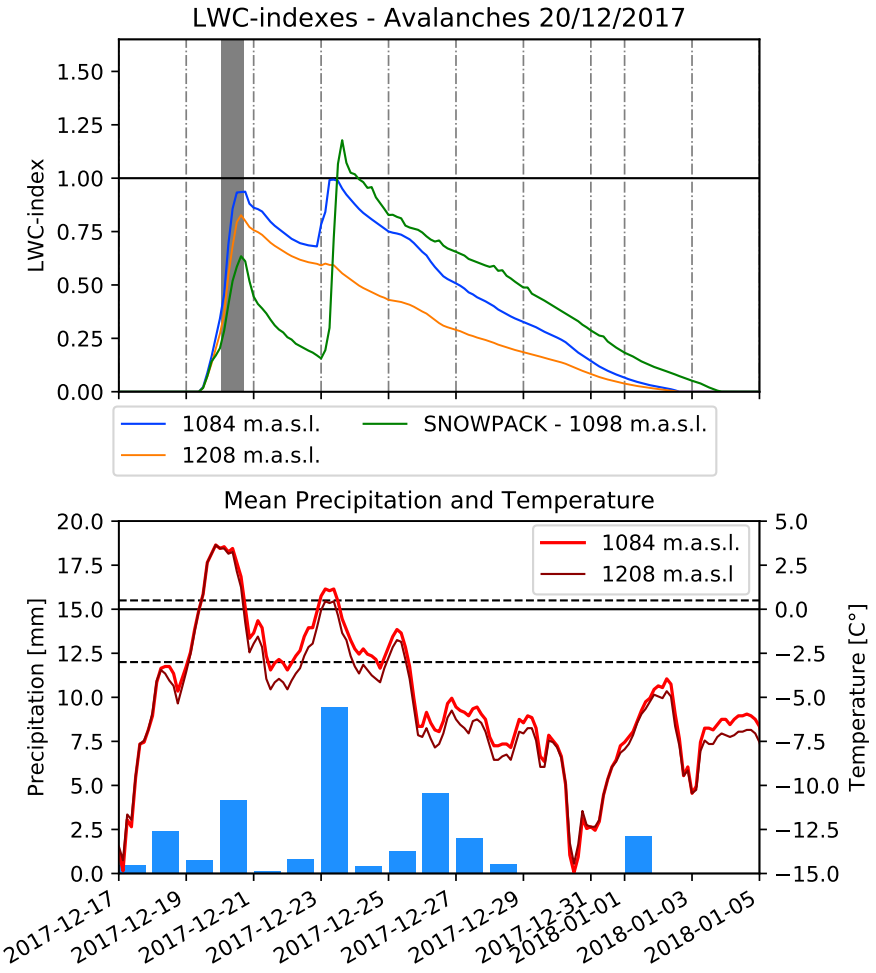

Figure 4.8: 1) LWC indexes for avalanches on 20/12/2017. The SNOWPACK model is run on point data with an elevation of 1098 m.a.s.l. which is approximately at the avalanches furthest north. The seNorge model uses the Xgeo grid (elevation 1084 and 1208 m.a.s.l.) data where the avalanches are located within the grid. The possible time of onset for the avalanches is shown as a grey bar.
2) The mean precipitation and temperature data from the two grid cells used to run the seNorge model. Daily summed precipitation is shown as blue bars, while temperature data is plotted every 3-hour in red lines. The two dotted black lines indicate the threshold air temperature for liquid or solid precipitation and possible temperature onset of melting in the model, on 0.5°C and −3°C respectively.

4.2 Wet-Snow Avalanche Activity in the Tromsø Region Compared to the LWC-index

4.2.1 2019 Avalanches

On 05/04/2019, 95 wet-snow avalanches are observed, divided into 29 lower and 29 upper 1x1 grid cells. When modeling the LWC index for all grid cells a pattern emerges. The LWC indexes in the grid cells below 250 m.a.s.l. shows little variation. The same occurs for the grid cells above 550 m.a.s.l. Figure 4.9 shows the mean LWC indexes together with mean precipitation and temperatures for these elevation ranges. The mean values are representative of the grid cells in these elevation ranges.

For the lower elevation grid cells, the LWC index has a sharp increase on 20/04 and passes maximum instability two weeks before the avalanches on 24/04. The higher elevation grid cells have an LWC index that has a sharp increase on 18/05, passing 1.0 on 21/05. When the index for the lower elevation grid cell rises the temperatures are for the most part positive, with around 7 mm of precipitation. The LWC index for the upper elevation grid cell gradually decreases in the same time frame. This is due to the temperatures at higher elevation being, for the most part, below -3°C, causing all precipitation to fall as snow and no melting occurring.

In the two weeks before the release of the avalanches, nearly every day has precipitation recorded for both elevation ranges. The threshold for liquid or solid precipitation at 0.5°C then becomes important to how the LWC index behaves. When temperatures are above this threshold, the precipitation is modeled as rain and the index will increase. Temperatures below this threshold have precipitation modeled as snow, causing the snowpack to increase and the LWC index to decrease. For the grid cells above 550 m.a.s.l., the temperatures are constantly below this threshold for the two weeks before the avalanches. For the lower elevation grid cells, the temperatures fluctuate around the threshold, causing the index to have the same fluctuations.

For all grid cells in the two elevation ranges (some are shown in the appendix), the days away from maximum instability have been checked. For the lower elevation grid cells, the LWC indexes pass maximum instability for the most part 13 and 14 days before the avalanches occur. For the higher elevation grid cells, the index rises mostly 16 and 17 days after the avalanches releases.

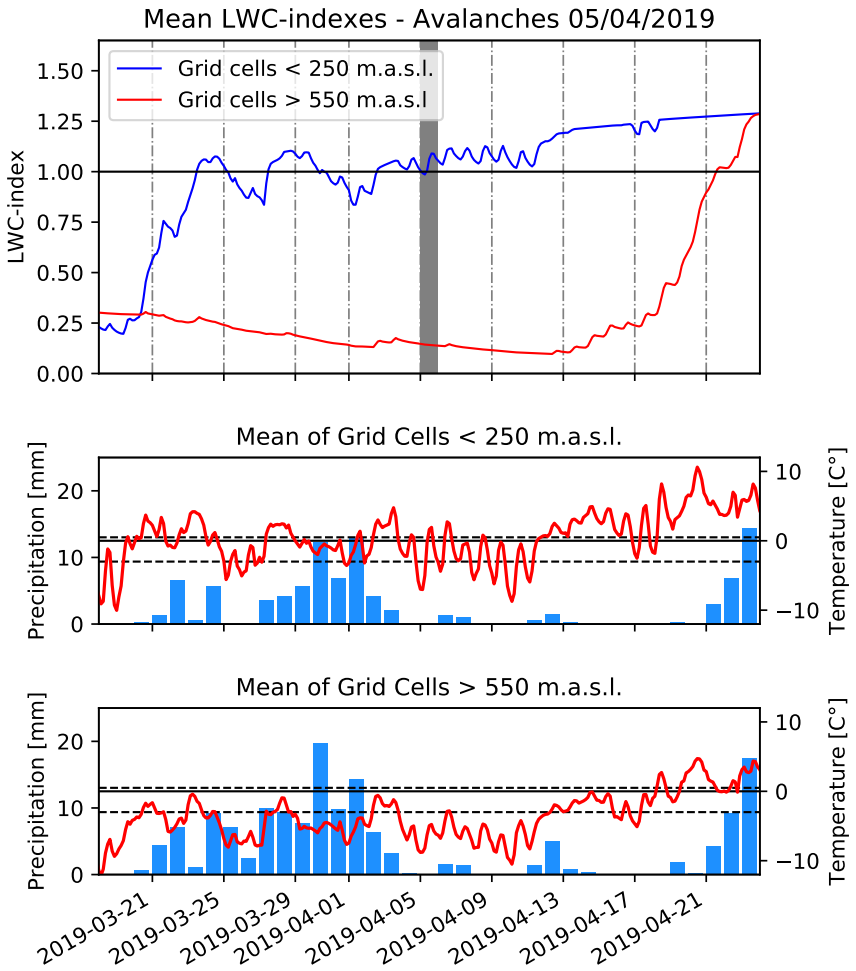

Figure 4.9: 1) LWC index for avalanches on 05/04/2019. The indexes are modeled from the average data of grid cells below 225 m.a.s.l. and above 550 m.a.s.l. and are representative of all grid cells in these elevation ranges. The possible time of onset for the avalanches is shown as a grey bar.
2) The mean precipitation and temperature data for grid cells in the two elevation ranges used to run the seNorge model. Daily summed precipitation is shown as blue bars, while temperature data is plotted every 3-hour in red lines. The two dotted black lines indicate the threshold air temperature for liquid or solid precipitation and possible temperature onset of melting in the model, on 0.5°C and −3°C respectively.

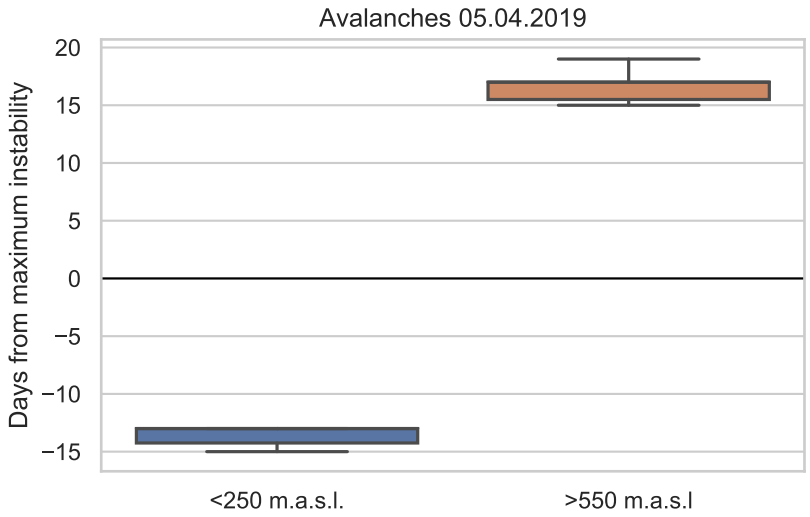

Figure 4.10: Box plots for LWC indexes passing maximum instability compared to the day of avalanche occurrence. 22 grid cells are below 250 m.a.s.l., while 25 grid cells are above 550 m.a.s.l. Negative values are LWC indexes hitting maximum instability n days before the avalanche. Positive values are n-days after the avalanches released. The elevation limits have been set based on where the LWC indexes show little variability between each other.

In the elevation range 250-550 m.a.s.l. it is harder to define sharp increases to the LWC indexes (and other patterns that are associated with wet-snow avalanche activity) in the time frame before the avalanches. Figure 4.11 shows the LWC indexes, temperature, and precipitation for 11 grid cells that are in this elevation range. The precipitation and temperature data are divided into minimum, maximum, and mean data. The LWC indexes are fluctuating much more in this elevation range, making it harder to define a clear-cut sharp increase that would indicate an onset of increased wet-snow avalanche activity. E.g., the index for the 296 m.a.s.l. passes maximum instability two days before the release of the avalanches but increased from an index level of 0.8. It also passes maximum instability eight days before the release of the avalanches, with an increase 13 days before that passes an index level of 0.8. As the temperatures fall with increasing elevation, the LWC indexes move toward being equal that of the grid cells above 550 m.a.s.l.

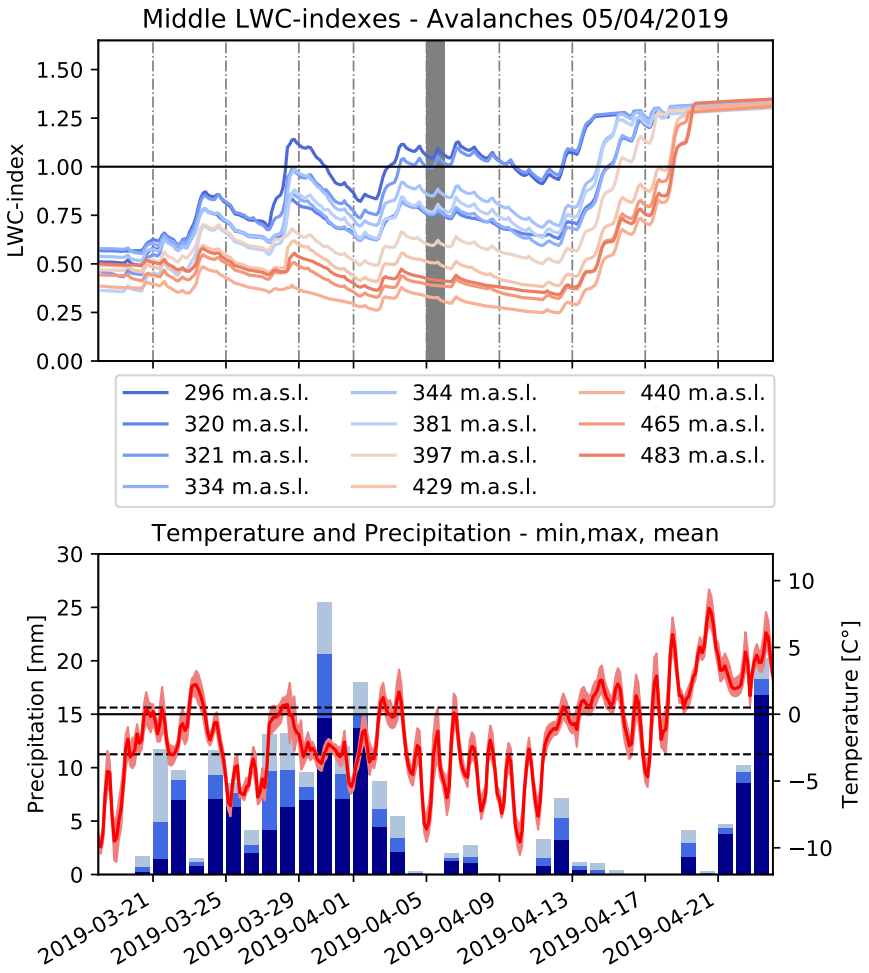

Figure 4.11: 1) LWC indexes for avalanches on 05/04/2019, in the elevation range 250-550 m.a.s.l. The possible time of onset for the avalanches is shown as a grey bar.
2) The minimum, maximum and mean precipitation and temperature data from the 11 grid cells used to run the seNorge model. Daily summed precipitation is shown as blue bars, while temperature data is plotted every 3-hour in red lines. The two dotted black lines indicate the threshold air temperature for liquid or solid precipitation and possible temperature onset of melting in the model, on 0.5°C and −3°C respectively.

4.2.2 2018 Avalanches

In 2018, only 10 wet-snow avalanches are registered. Eight of them are in Brokskaret on 17/04, with four on the western slope of Gråtinden and four on the eastern slope of Tverrfjellet. The last two avalanches released on 13/04 at the slope of Tverrbotnfjellet in Lavangsdalen.

The LWC indexes for the avalanches in Broksakeret are shown in figure 4.12 and figure 4.13. The indexes have a sharp increase and pass 1.0 before it flattens out. This makes it easy to the define onset of wet-snow avalanche activity from these indexes. The precipitation registered for these grid cells are close to equal, and the difference in temperature is what causes them to increase at slightly different times. The temperatures shift downwards as the elevation increases. This causes the precipitation that falls from 06/04-12/04 to fall as rain for the grid cell on 211 m.a.s.l. and as snow for all other grid cells. The increase to the LWC index starts five days earlier for the lowest grid cell as a result of this difference. When the sharp increase to the LWC indexes occurs on 13/04, there are no precipitation recorded and a sudden increase to the temperature to above 5°C occurs. From this day until the avalanches release, the temperatures have daily fluctuations, staying above 0°C for the most part, and no precipitation is recorded.

The LWC indexes for the two grid cells on the east-facing slope of Tverrbotnfjellet is shown in figure 4.14 together with the temperature and precipitation data. These two grid cells have a much larger elevation difference than those in Brokskaret. The recorded precipitation is equal for the two grid cells, with temperatures showing large variations as a result of the elevation differences. From 05/04, the lower grid cell has an LWC index that increases with diurnal fluctuations. The daily temperatures are above the threshold for rain, with nightly temperatures being below. This is the reason for fluctuations in the index. The upper grid cell does not have temperatures above the onset of melting, meaning all precipitation falls as snow and no melting is recorded. When the LWC index for the upper grid cell starts to rise, no precipitation is recorded and a sudden spike in the temperature to above 5°C is recorded. Table 4.2 shows how many days differ between avalanches releasing and LWC indexes hitting maximum instability.

Mountain	Avalanche Count	Grid Cell (elevation)	Before (-) or After (+) maximum instability on LWC-index
Gråtinden	4	Lower (378) Upper (554)	+2 +1
Tverrfjellet	4	Lower (211) Upper (557)	+5 +1
Tverrbotn-fjellet	2	Lower (131) Upper (853)	+2 - 3

Table 4.2: Difference in days between avalanches releasing and LWC indexes hitting maximum instability for the 2018 wet-snow avalanches. All 2018 avalanches occurred within the four days from 13.04 to 17.04.

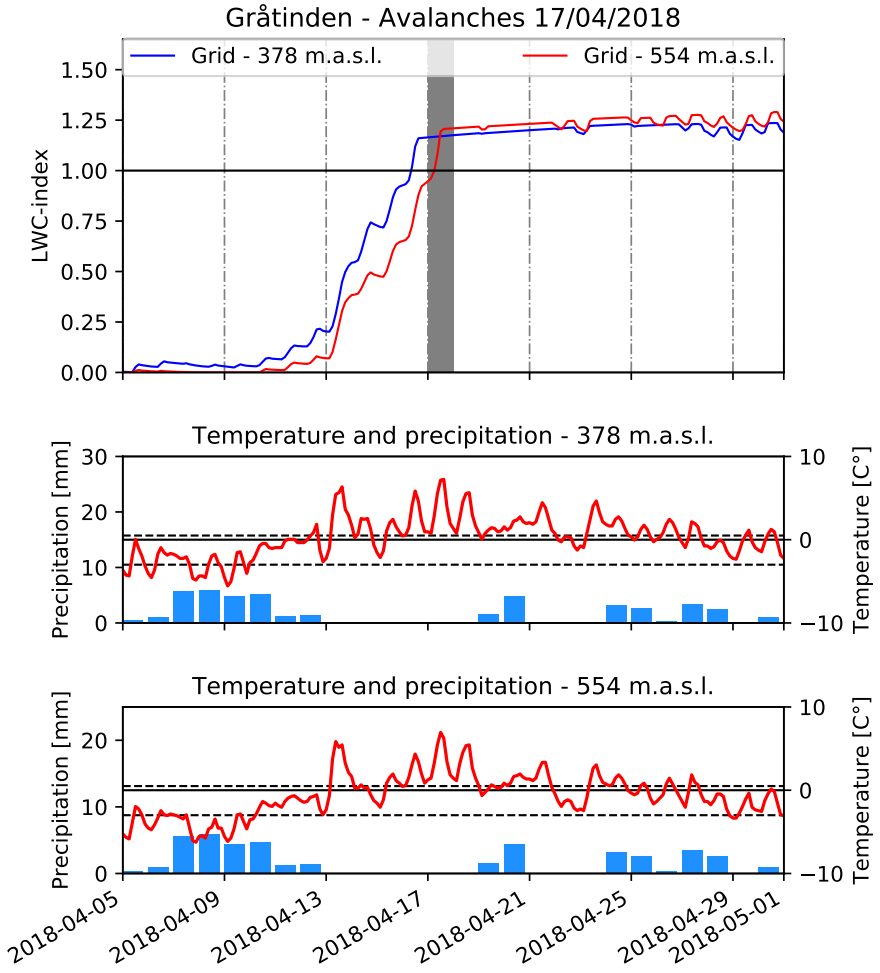

Figure 4.12: 1) LWC indexes for the two grid cells on the east-facing slope of Gråtinden. The possible time of onset for the avalanches occur at 17/04 and are shown as grey bars.
2) The precipitation and temperature data for the two grid cells used to run the seNorge model. Daily summed precipitation is shown as blue bars, while temperature data is plotted every 3-hour in red lines. The two dotted black lines indicate the threshold air temperature for liquid or solid precipitation and possible temperature onset of melting in the model, on 0.5°C and −3°C respectively.

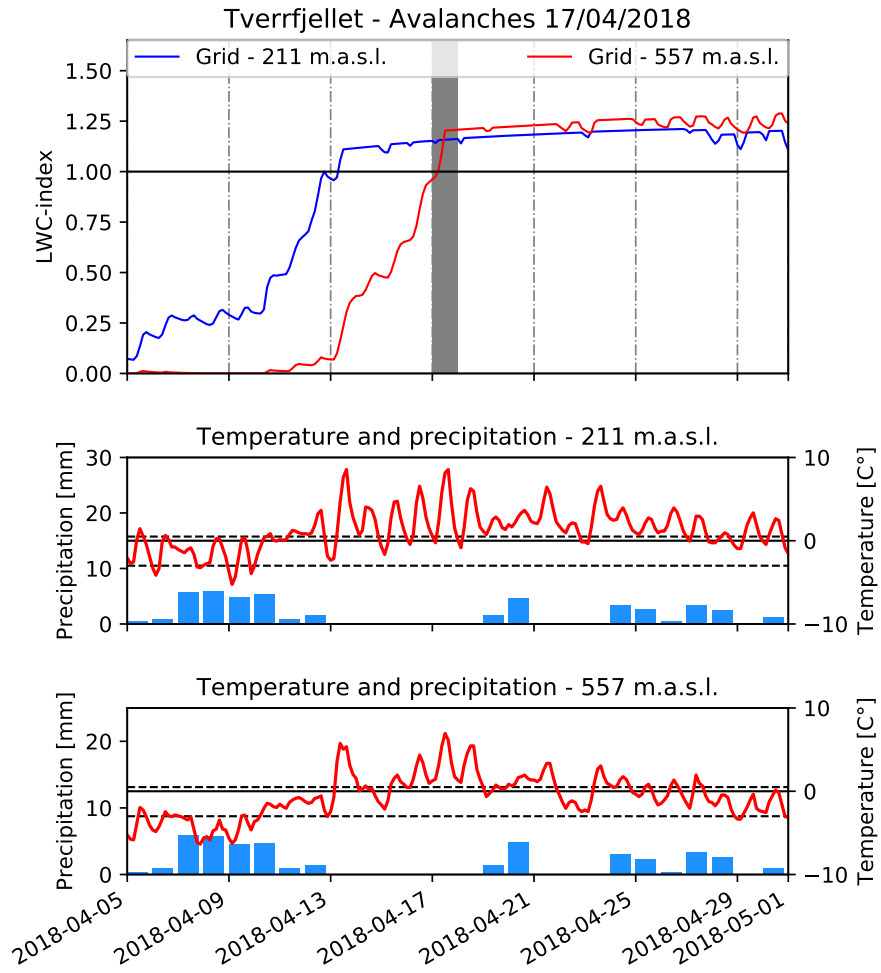

Figure 4.13: 1) LWC indexes for the two grid cells on the east-facing slope of Tverrfjellet. The possible time of onset for the avalanches occurs on 17/04 and is shown as a grey bar.
2) The precipitation and temperature data for the two grid cells used to run the seNorge model. Daily summed precipitation is shown as blue bars, while temperature data is plotted every 3-hour in red lines. The two dotted black lines indicate the threshold air temperature for liquid or solid precipitation and possible temperature onset of melting in the model, on 0.5°C and −3°C respectively.

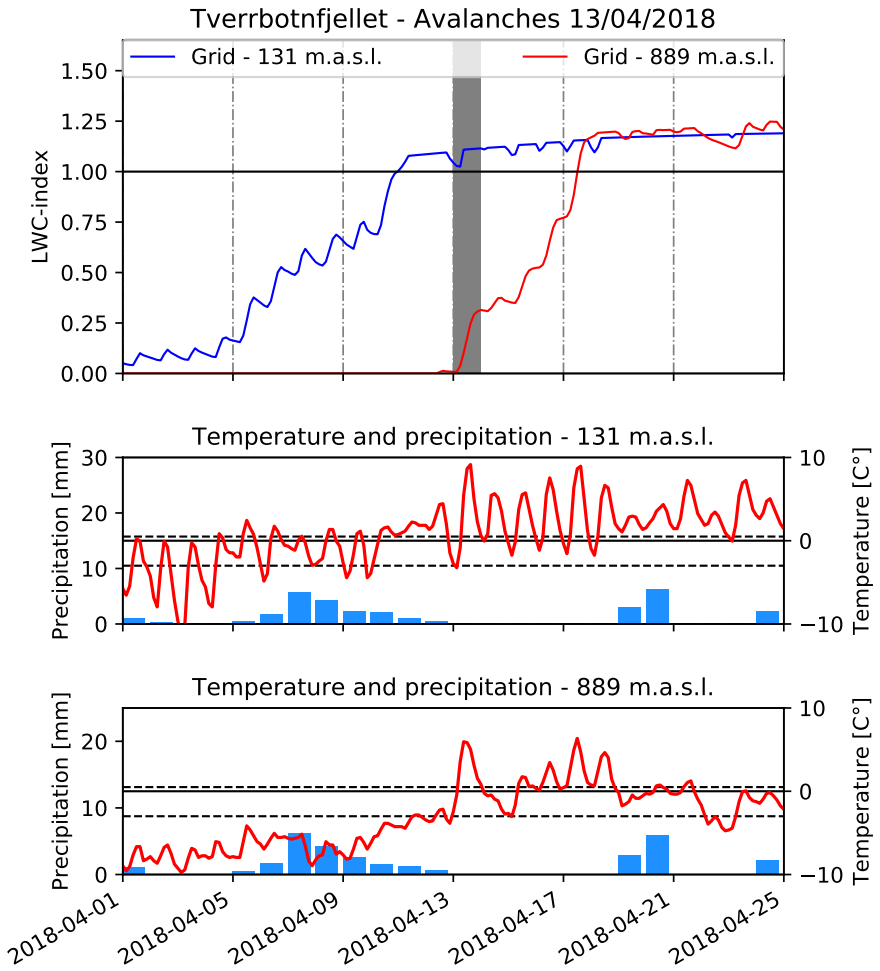

Figure 4.14: 1) LWC indexes for the two grid cells on the east-facing slope of Tverrbotnfjellet. The possible time of onset for the avalanches occurs on 13/04 and is shown as a grey bar.
2) The precipitation and temperature data for the two grid cells used to run the seNorge model. Daily summed precipitation is shown as blue bars, while temperature data is plotted every 3-hour in red lines. The two dotted black lines indicate the threshold air temperature for liquid or solid precipitation and possible temperature onset of melting in the model, on 0.5°C and −3°C respectively.

4.2.3 2017 Avalanches

Sixty wet-snow avalanches are registered in 2017. These avalanches occur in three different periods; early February, mid-March, and mid-April. Over half of the 2017 avalanches were released on 22/03/2017. Figure 4.15 shows the LWC indexes for every grid cell below 500 m.a.s.l. The indexes are divided into two elevation groups: elevation below 200 m.a.s.l. and elevation between 250-500 m.a.s.l., and the minimum, maximum, and mean temperature and precipitation are shown for each group. For the grid cells above 500 m.a.s.l. the LWC indexes show no increase due to temperatures being too low.

All indexes increase sharply from a low point on 13/04, and the lower elevation grid cells pass maximum instability around 15/03 and 16/03. This pattern gradually flattens out as the elevation increases, with the grid cells closest to 500 m.a.s.l. having an index increasing only to around 0.5. As the LWC indexes start to increase no precipitation is recorded. The temperatures are increasing towards 5°C for the lowest elevation grid cells and around 2°C for the highest elevation grid cells.

After the indexes reach their peaks around 16/03, they gradually decrease until the avalanches releases on 22/03. Precipitation is falling and temperatures are decreasing below 0°C for all grid cells during the decrease. No precipitation is recorded from 20/03 to 22/03, and for the lower elevation grid cells temperatures increase to around 0.5°C in this period. This causes the LWC indexes for grid cells below 200 m.a.s.l. to have a small increase from around 0.6 to 0.9 in this period.

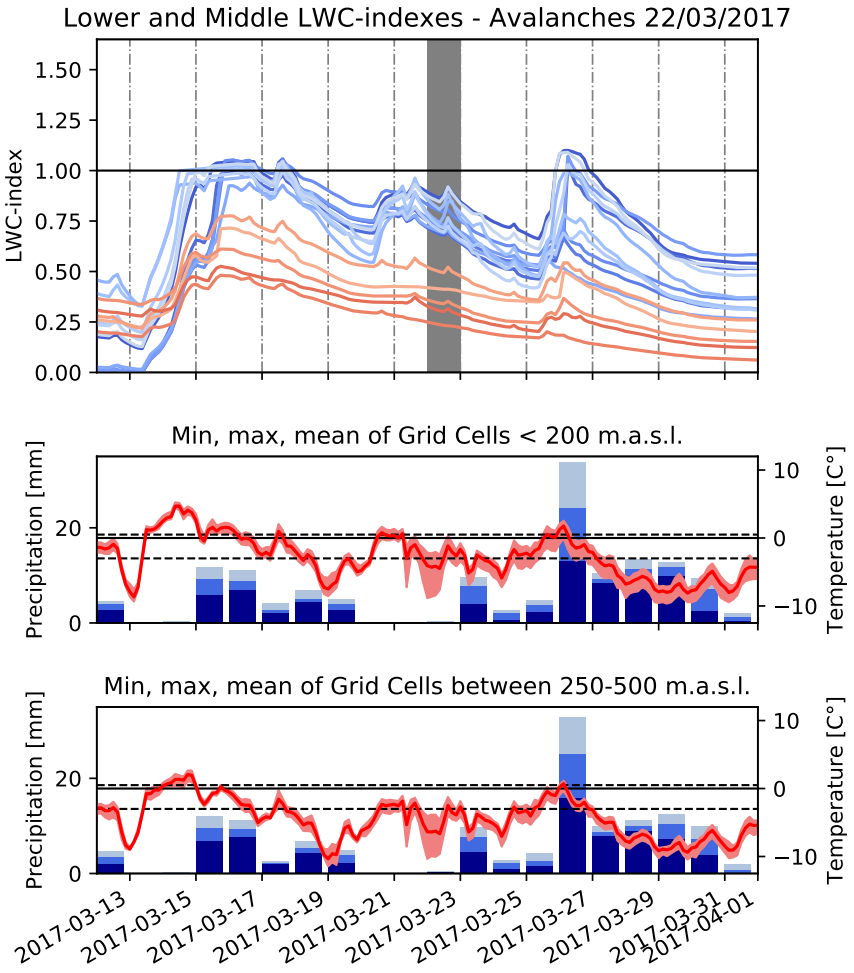

Figure 4.15: 1) LWC indexes for the grid cells below 500 m.a.s.l., divided into two elevation groups. Shades of blue are indexes below 200 m.a.s.l. and shades of red are indexes from grid cells between 250-500 m.a.s.l. Darker color shading is towards the highest elevation in the respective group. The possible time of onset for the avalanches is shown as a grey bar.
2) The minimum, maximum and mean precipitation and temperature data the grid cells in each elevation group used to run the seNorge model. Daily summed precipitation is shown as blue bars, while temperature data is plotted every 3-hour in red lines. The two dotted black lines indicate the threshold air temperature for liquid or solid precipitation and possible temperature onset of melting in the model, on 0.5°C and −3°C respectively.

Four avalanches were released on 02/02/2017. Figure 4.16 shows the LWC indexes for the two mountains the avalanches occurred on, both lower and upper grid cells, with their respective temperatures and mean precipitation. The LWC indexes start to increase eight days before the avalanches release. The lower elevation grid cells have indexes with sharp increases that nearly reach or reach maximum instability. The higher elevation grid cell starts to increase two days later, and only reaches an index level of 0.2. In the period where the LWC indexes increases, over 10 mm of precipitation is recorded, and temperatures increase towards 5°C for the lower grid cells. As the elevation increase, the temperatures decrease. This causes more and more of the precipitation to be modeled as snow with higher elevation.

The LWC indexes start to decrease three days before the release of the avalanches, with temperatures rapidly falling below −3°C for all grid cells. The temperatures stay below this threshold for the most part until the avalanches release. On the day of the avalanches, there is no precipitation, with temperatures rising above the threshold for the onset of melt. However, since the temperatures are around −3°C for both grids the incoming shortwave radiation is not high enough for much melting to occur in February. This only causes the index to slow the rate of the decrease on the day of the avalanches.

In April, 21 avalanches were released on the east-facing slopes of the two mountains, Rypedalsaskla and Stortinden. The LWC indexes, temperatures and mean precipitation for the grid cells on these mountains are shown in figure 4.17. For the lower grid cells, the LWC indexes increase sharply on 03/04, and the lowest elevation passes maximum instability a day later. This is 11 and 13 days before the avalanches occurred. All the indexes start to decrease on 05/04 and continuously decreases until the release of the avalanches. On the day of the index increase, around 5 mm of precipitation is recorded. The temperatures are above the threshold for liquid precipitation for the lower grid cells, and below for the two high elevation grid cells. The LWC indexes for the higher elevation grid cells do not increase, as a consequence of the snowpack increasing in height from solid precipitation, and the melt rate is lower than this increase. From 05/04 there are negative temperatures for all grid cells until the release of the avalanches. Ten and 12 days with temperatures between −3°C and below −10°C suggest that the avalanches might be categorised wrong as wet-snow avalanches. It might also be that water-induced tensile cracks have formed with the glide-snow avalanche releasing several days later.

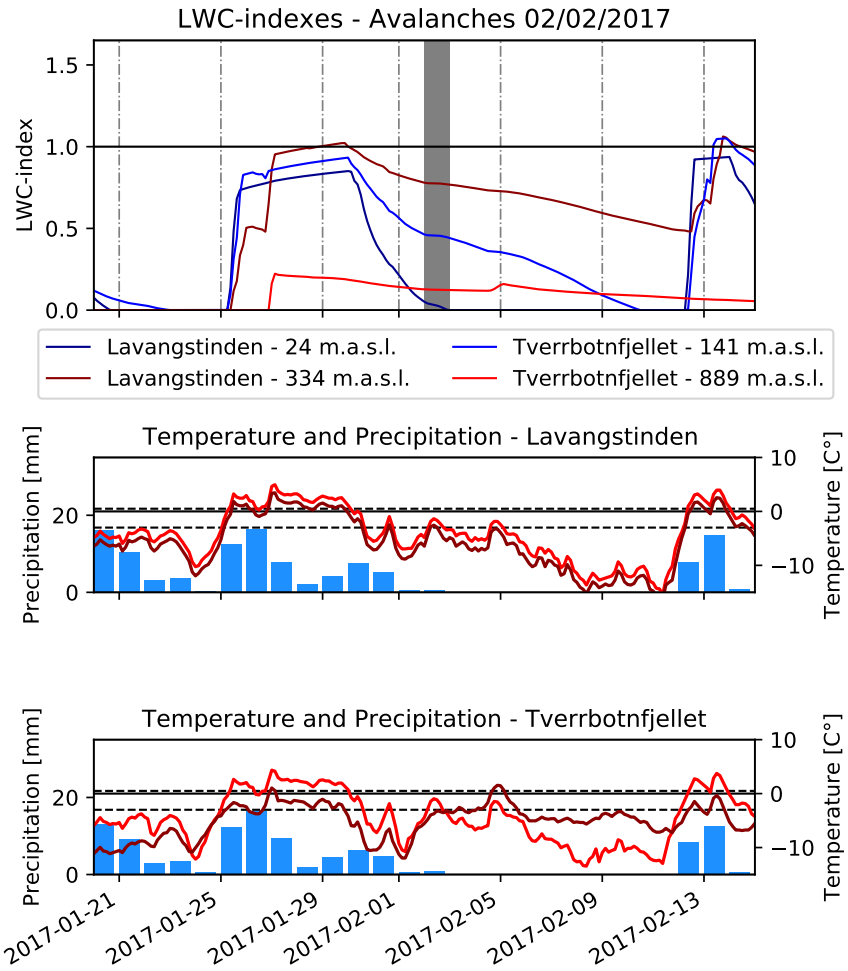

Figure 4.16: 1) LWC indexes for two grid cells on Tverrbotnfjellet and two grid cells on Lavangstiden.The possible time of onset for the avalanches is shown as a grey bar.
2) The precipitation and temperature data for the four grid cells used to run the seNorge model. Daily summed precipitation is shown as blue bars, while temperature data is plotted every 3-hour in red lines (dark red is the highest elevation grid cell). The two dotted black lines indicate the threshold air temperature for liquid or solid precipitation and possible temperature onset of melting in the model, on 0.5°C and −3°C respectively.

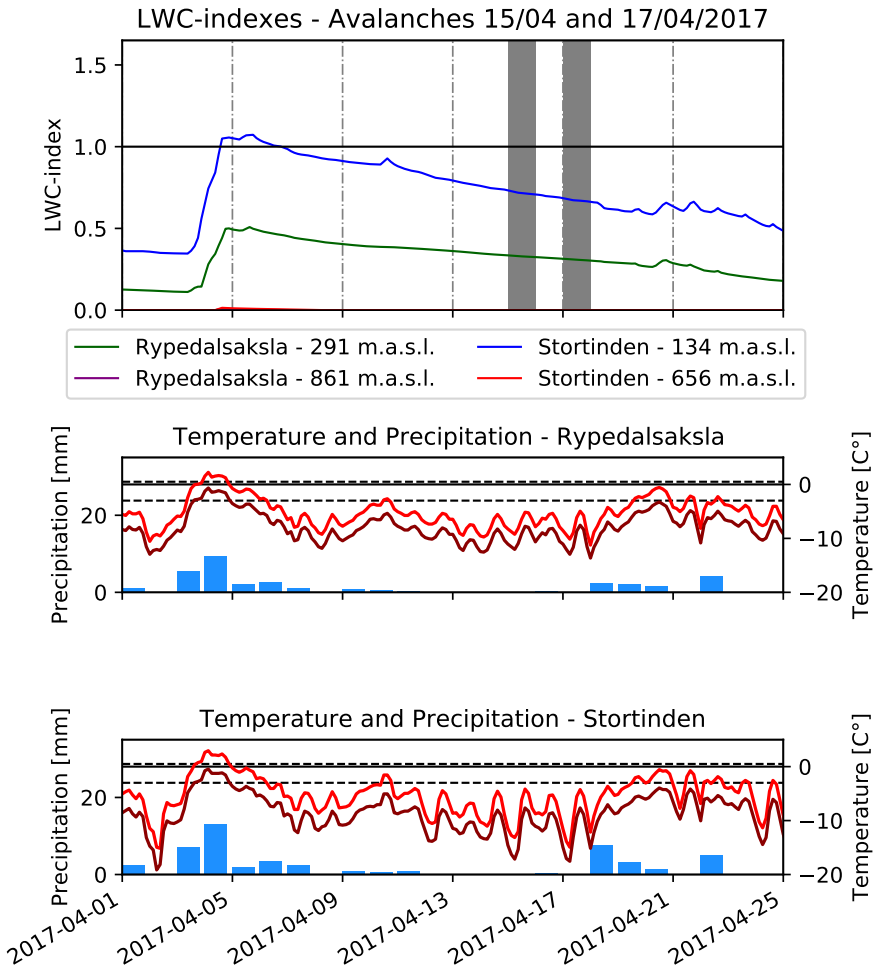

Figure 4.17: 1) LWC indexes for two grid cells on Rypedalsaskla and two grid cells on Stortinden.The possible time of onset for the avalanches is shown as a grey bar.
2) The precipitation and temperature data for the four grid cells used to run the seNorge model. Daily summed precipitation is shown as blue bars, while temperature data is plotted every 3-hour in red lines (dark red is the highest elevation grid cell). The two dotted black lines indicate the threshold air temperature for liquid or solid precipitation and possible temperature onset of melting in the model, on 0.5°C and −3°C respectively.

4.2.4 2015 Avalanches

In Lavangsdalen and Smalakdalen, 22 avalanches are observed in 2015 (13 on 08/01 and nine on 04/05). High mountains with steep slopes cause the upper grid cells to be around 700 m.a.s.l. and upwards while the lower grid cells are around 350 m.a.s.l and lower.

The LWC indexes for the higher grid cells around the avalanches occurring on 04/05/2015

For the avalanches occurring on 04/05/2015, the LWC indexes for the higher grid cells are shown in figure 4.18. The indexes show the same trend as in 2019. Around two weeks before the release of the avalanches, the lowest elevation grid cells start to rise and passing maximum instability. Those higher up stays relatively flat and the increase comes after the release of the avalanches. When the lower grid cell increases, several days with precipitation around 5 mm is recorded. The temperatures are just around the threshold for solid and liquid precipitation for all grid cells. This causes the precipitation to be modeled as rain for the lowest elevation and as snow for the highest elevations. After the initial increase, the temperatures vary between 0°C and −5°C until 04/05, and no precipitation is recorded. After 04/05 the temperatures rapidly increase towards 5°C, causing the indexes for the higher elevation grid cells to increase. For the grid cells below 250 m.a.s.l., the snow cover melts around 21/04, giving no index values after that point (shown in the appendix).

For the avalanches in January, the LWC index does not pass maximum instability for any of the grid cells. Figure 4.19 shows the indexes for all grid cells together with temperature and mean precipitation data. From 29/12/2014 to 01/01/2015 around 40 mm of precipitation is recorded. In the same period, the temperatures increase, and on 30/12/2014 all grid cells have temperatures above 0.5°C. For the lowest grid cells, the temperatures stay above this threshold until 02/01/2015, and all precipitation fall as rain. As the elevation increases, the temperatures decrease and fall below the threshold for liquid precipitation at one point. This causes the LWC indexes for the lower grid cells to sharply increase and flatten out, while the higher elevation grid cells have an increase in two phases.

The temperatures rapidly decrease from around 3°C on 02/01 to below −5°C on 05/01, causing all indexes to decrease. Only the grid cells under 150 m.a.s.l. have a new increase to the indexes on the date of the avalanches, with the lowest grid cell having an index peaking at 0.82 on the day. This increase occurs due to the fact that the temperature for these grid cells has a daily increase above 1°C, and around 2.5 mm of precipitation is recorded. After the indexes peaks on 08/01, it rapidly decreases again as a result of temperatures dropping to negative values during the night. For the higher elevation grid cells, the temperature stays negative throughout the day, and no increase to the volumetric water content occurs.

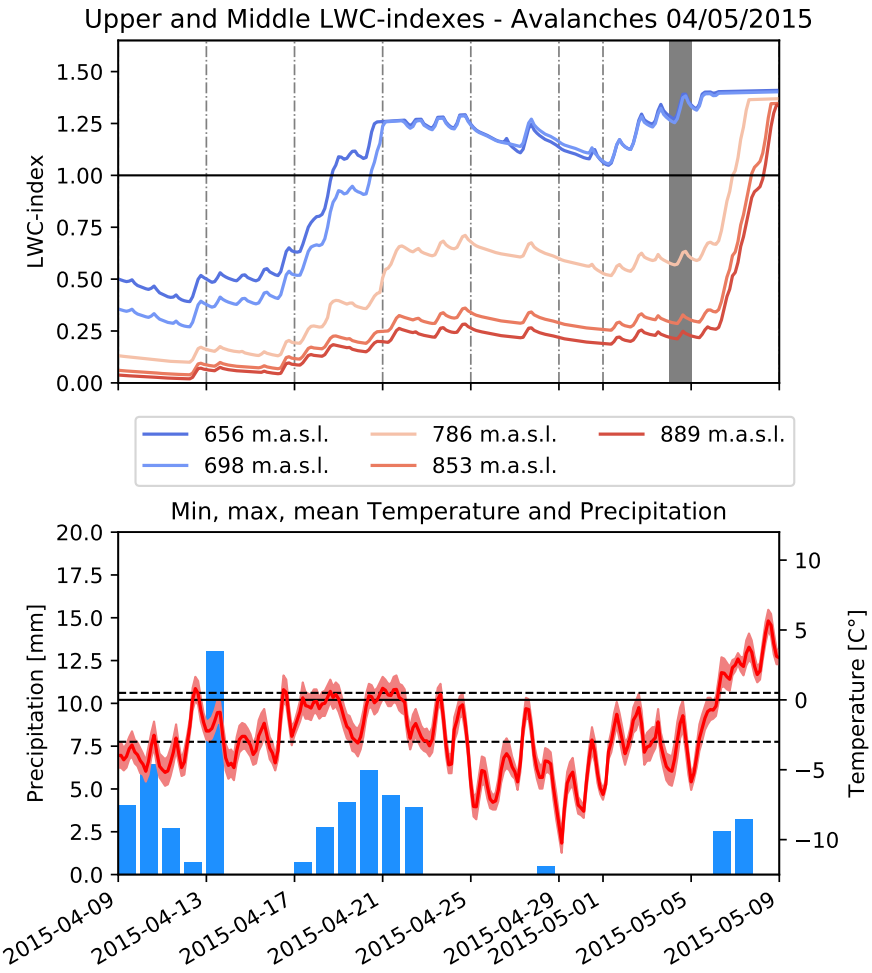

Figure 4.18: 1) LWC indexes for five grid cells above 650 m.a.s.l. in Smalakdalen and Lavangsdalen. The possible time of onset for the avalanches is shown as a grey bar.
2) Minimum, maximum and mean temperature data, and mean precipitation data for the five grid cells used to run the seNorge model. Daily summed precipitation is shown as blue bars, while temperature data is plotted every 3-hour in red lines (light red is min and max values). The two dotted black lines indicate the threshold air temperature for liquid or solid precipitation and possible temperature onset of melting in the model, on 0.5°C and −3°C respectively.

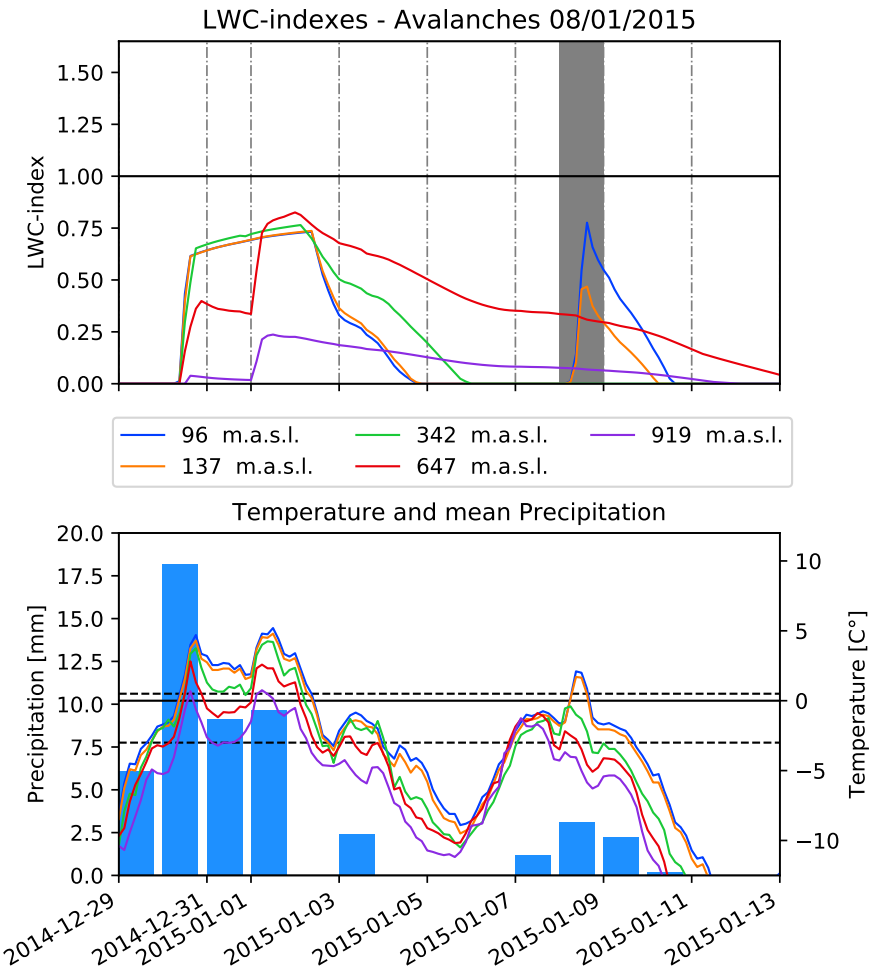

Figure 4.19: 1) LWC indexes for five grid cells in Lavangsdalen and Smalakdalen. The possible time of onset for the avalanches is shown as a grey bar.
2) Mean precipitation data and temperatures data for all grid cells used to run the seNorge model. Daily summed precipitation is shown as blue bars, while temperature data is plotted every 3-hour. The two dotted black lines indicate the threshold air temperature for liquid or solid precipitation and possible temperature onset of melting in the model, on 0.5°C and −3°C respectively.

CHAPTER 5

Discussion

5.1 SeNorge Model Performance on Kyrkjestølen

Modeled SD and SWE Compared to Station Data

The seNorge model underestimated the SD and SWE compared to the observed station data on Kyrkjestølen (figure 4.1). For both years there were certain times when the observed SD and SWE rapidly increased without the recorded precipitation matching such high values. A reasonable assumption is that undercatch of the precipitation (or a faulty gauge) caused this discrepancy between measured SWE and observed precipitation. Thus, the seNorge model underestimates the SWE and SD as a result of precipitation being too low. A simple procedure of adding a constant factor to the solid precipitation made the modeled values approach the observed values. A constant value of 1.50 to 2.40 throughout the whole winter season was needed to have reasonable results for the SD and SWE. Owing to the the simplicity of this approach, a good modeled fit throughout the entire winter season was not possible. However, looking at the times when the model values are matching well, the rate of accumulation and melting of the snow matches that of the station. Consequently, the seNorge snow model will give reasonable results if the precipitation data are correct.

Modeled Liquid Water Content Index on Kyrkjestølen

The timing of melting and refreezing of the snowpack is not affected by the amount of solid precipitation. As seen in equations 2.2 and 2.3, the timing is based on T_a. By only adjusting solid precipitation to get a higher modeled SD and SWE, the LWC indexes rise and fall simultaneously with different rates (Figures 4.3, 4.4, and 4.5). Higher snow depths increase and decrease slower than low snow depths due to the index being based on volumetric liquid water content. When analysing the timing of LWC indexes indicating a higher probability of wet-snow avalanche activity, this mostly had an impact in early winter. A common occurrence in December and January was warm weather coming in short bursts (figure 4.5). During such short melting cycles, the LWC index would not always reach maximum instability. Thicker snowpacks were then observed to peak at a lower index level.

In spring the general trend for the LWC indexes was to reach maximum instability and then flatten out. The indexes can then stay high because of continuous melting conditions or decrease again when conditions for refreezing

takes over. If the melting period is long enough for all indexes to pass maximum instability, the observed delay was at most two days between the highest and lowest SD (figure 4.3). At times, the indexes did not start to melt from the same index level due to snowpacks with higher SD needing more time to fully refreeze. This was seen in May 2017 where the LWC index started to increase from 0 for the original seNorge output, and from 0.5 when a factor of 2.40 was added to the solid precipitation. However, since the lower modeled SD had an LWC index that increased faster, they passed maximum instability at the same time.

An inaccurate modeled SD will have an LWC index that either rises too slow or too fast. If the index rises too fast, it will show an unstable snowpack earlier than intended and avalanche activity can then occur later than expected. However, since the LWC index is unable to indicate when the snowpack has stabilised from metamorphism (Mitterer, Techel et al., 2013), this will only extend the set time frame of how many days increased avalanche activity is expected after the index passes 1.0. By increasing this time frame by two days, underestimations of SD and SWE will give the same indications of increased probability of wet-snow avalanche activity as a correct modeled SD/SWE. Also, if the modeled SD/SWE is underestimated, the snow will completely melt earlier in the model than in reality. As a consequence, the model may fail to predict avalanches late in the winter season, since a melted modeled snowpack do not produce an LWC index.

If the SD/SWE is modeled to high, the LWC index will rise slower than if it was modeled accurately. This could cause avalanches to release while the LWC index rises without reaching a level where higher activity of wet-snow avalanches is expected. Since sharp increases to the LWC index were clearly associates with increased avalanche activity (Bellaire et al., 2017), this will only cause problems if the modeled SD is magnitudes thicker than the real SD. In such cases, the modeled LWC index will barely show an increase in comparison to the real situation.

Overall, a modeled SD that does not match with the real situation will still show outline of an LWC index that is associated with higher avalanche activity when wet-snow avalanches release. Some inaccuracies should be taken into considerations when analysing the LWC index against wet-snow avalanche activity such as the index level not rising to the expected level and avalanches releasing later than expected. However, other problems like avalanches releasing at times when the LWC index is decreasing will not be associated with under- or overestimations of the modeled SD.

5.2 Modeled LWC-indexes Compared to Avalanche Activity at Tyin

Since the precipitation data on Kyrkjestølen did not match the accumulation of snow, the modeled SD is smaller than reality for the SNOWPACK model. For the 16/17 winter season, the seNorge modeled snowpack was closest to reality, while this was reversed for the 17/18 winter season. A comparison between the models' LWC indexes were performed with the original solid precipitation data as a consequence of the SNOWPACK model only being run on this data.

All avalanches at Tyin released within a small area on east-facing slopes. This caused the interpolated precipitation and temperature data in grid cells to be equal and only change with elevation. Consequently, the LWC index for the seNorge model only changed with elevation within this avalanche area. For the SNOWPACK model, the given point was at the avalanches furthest north. This point was used to model the LWC index for all avalanches with the assumption that the SNOWPACK model would not change significantly within this area. With this assumption, the avalanches farthest away from the SNOWPACK point had a larger uncertainty to the LWC index than the avalanches that were closer.

In spring 2017, the LWC indexes for both the seNorge model and the SNOWPACK model increased at the same time with diurnal fluctuations (figure 4.6). The difference in amplitude was caused by a much thicker snowpack for the seNorge model. The grid cell data showed no precipitation and high daily temperatures in the period where the indexes increased. The LWC index for the SNOWPACK model ended on 07/05 due to the complete melting of the snowpack. For the seNorge model, the avalanches released two weeks after the LWC index flattened out, which should in theory be enough time to stabilise the snowpack. However, the new added load from the 18 mm of rain throughout the day may have caused critical instabilities.

For the 2018 spring avalanches, the seNorge model had LWC indexes that showed increasing wet-snow avalanche activity at the optimal time (figure 4.7). The wet-snow avalanches released within 0-6 days of the index passing maximum instability. The increase of the LWC index was caused by high temperatures without any precipitation recorded. Originally, these conditions were showing the best results for the SNOWPACK model together with high values of shortwave radiation (Mitterer, Techel et al., 2013). However, the LWC index for the SNOWPACK model at Tyin did not match well with the wet-snow avalanche activity. The index did not start to increase until the third day of avalanche activity, and then it only registered a level of 0.25. At the fourth day of avalanches, the index peaked at 0.7. Even though the SD for the seNorge model is much smaller than for the SNOWPACK model at this time (figure 4.1), the seNorge model follows the trend of the station data better. The reason for this can only be hypothesised due to missing information about the SNOWPACK model input. The radiation for the seNorge model does not use any cloudiness information and assumes clear-sky radiation. As there was no precipitation at the time, it is reasonable to assume clear sky, and the modeled radiation would therefore have matched well with the actual radiation. The SNOWPACK model, on the other hand, may have had shortwave radiation not

matching well with the actual conditions, which would explain why the LWC index for the SNOWPACK model did not match well.

The avalanches in December 2017 were the only early winter season avalanches observed at Tyin. At the day of the avalanches all LWC indexes had a sharp increase, but without reaching 1.0. This was associated with increased wet-snow avalanche activity (Bellaire et al., 2017). The sharp increase occurred as a result of high temperatures reaching nearly 5°C. Both the seNorge model and SNOWPACK model had LWC indexes that showed the same trend at the same elevation, only peaking at different levels. The reason this was the only time the two models' LWC index matched fairly well was probably because the modeled SD of the two models were much closer to each other at this time than in spring. This suggest that the LWC indexes for the two models matches closely if the SD is equal and following the same trend.

Overall, for the avalanches around Tyin, the LWC index for seNorge model indicated the wet-snow avalanche activity better than the LWC index for the SNOWPACK model. The differences between the two indexes seemed to come from the increasing differences in snow depth. The results showed that at times when the index increases due to temperatures rapidly increasing to above 1°C, the seNorge model can predict higher levels of wet-snow avalanche activity well. However, the index did not indicate a time frame for when the snowpack would stabilise after passing 1.0. These results matched well with the original finding of Mitterer, Techel et al., 2013.

5.3 Evaluation of LWC-index Compared to Wet-Snow Avalanche Activity in the Tromsø Region

The avalanches were spread out over a larger area in Tromsø than in Tyin. The interpolated precipitation and temperature data still varied mostly with elevation in this larger area. Consequently, the LWC indexes varied mostly with elevation. All the avalanches were on either east, west or south facing slopes. If the elevation of the grid cells were equal, the difference in aspect did not affect the LWC index significantly. Taking the mean of all LWC indexes from grid cells in the same elevation range could therefore produce a representative LWC index for that specific elevation range.

There were some avalanches in the Tromsø region that matched well with LWC index levels associated with increased avalanche activity. These were the avalanches on 17/04/2018 (figure 4.12 and 4.13). The differentiating factor for these avalanches was that no precipitation had been recorded when the LWC index increased as a result of a rapid rise in temperature to above 5°C. The same conditions were found for the April 2018 avalanches at Tyin which also matched well with increased avalanche activity (figure 4.7). Since the avalanches occurred in April, the modeled shortwave radiation was high. These are the same conditions that were found to have the best results in the regional LWC index analysis in Switzerland (Mitterer, Techel et al., 2013).

The LWC index for the avalanches that released on 13/04/2018 works well at lower elevations, while the index for the higher grid cell increases three days too late (figure 4.14). Before the avalanches on 13/04, a small amount of

precipitation was recorded. For the lower elevation grid cell, the temperatures fluctuated diurnally with high temperatures in the day. This caused most of the precipitation to fall as rain with continuous melting in daytime. When looking at elevations above 880 meters, the temperatures never passed the onset of melting. As a result, all precipitation was modeled as snow at this altitude. On the day with the avalanches, there was a large spike in the temperature. This could have been the triggering factor, and both grid cells recorded temperatures above 5°C. The LWC index for the lower elevation grid cell showed a snowpack that was already unstable when this occurred, while for the high elevation grid cell this was the first day of melting in the model. The LWC index for the higher grid cell did not give the same indication of wet-snow avalanche risk as the lower grid cell did at this date. This shows an important elevation dependency when modeling the LWC index.

Since the LWC index indicates wet-snow avalanche risk for a given elevation range, problems occur when avalanches releases on an elevation far from the elevation of the grid cells. In Tromsø, the elevation differences between two neighbouring grid cells were often very large. As a result, the LWC index was only modeled for a high elevation and a low elevation grid cell on a mountain. Given that the LWC index mostly changed with elevation, a solution to this problem could be to include all grid cells within a set radius of a location. The indexes within this circle could be summarised, giving index values for many different grid cell elevations. This would give a regional indication of wet-snow avalanche activity at different elevation ranges.

A sharp increase of the LWC index without reaching a value of 1.0 was associated with increased avalanche activity in Bellaire et al., 2017. This was especially seen early in the winter season. For the avalanches in January 2015, the lower elevation grid cells had LWC indexes showing this pattern (figure 4.19). A sharp increase to the index occurred due to a daily temperature spike above 1°C in conjunction with small amounts of precipitation. This was also seen for the early season avalanches at Tyin (fiugre 4.8), which indicates that the LWC index in the seNorge model can show increased probability for wet-snow avalanches in early winter seasons if the temperatures passes 1°C combined with some precipitation.

Most of the avalanches did not match well with a time where the LWC index indicated high avalanche activity based on the findings in the SNOWPACK model. Many of these situations had precipitation recorded with the temperatures varying around 0°C for several days before the release of the avalanches. This caused the LWC index to rise with the precipitation for the lower grid cells as it was above the threshold for rain. For the higher grid cells, this threshold temperature was not reached, causing the index to gradually fall due to higher snow depth from solid precipitation. This was seen for the avalanches in 2019 and spring 2015 (figure 4.9 and 4.18). Some amount of precipitation was recorded continuously several weeks before the release of the avalanches, and as a result, the LWC index rose either too early or not at all depending on the elevation of the grid cell. None of these LWC indexes showed a clear indication of high avalanche activity just before the avalanches occurred, and this seems to be a recurring issue when there is a longer period with continuous precipitation before the release of the avalanches. This issue

may have been caused as a consequence of the precipitation being miss-classified when the temperatures are fluctuating around the threshold for solid and liquid precipitation.

Some of the avalanches occurred at times where the LWC index was decreasing. This contradicts the findings in Bellaire et al., 2017 that a decreasing LWC index is associated with periods without avalanche activity. This was seen in March and February 2017 (figure 4.15 and 4.16). Temperatures for the lower elevation grid cells were just below the threshold for solid or liquid precipitation at the time of the avalanches. A misclassification of the precipitation could have caused the index to decrease when in reality the liquid water content increased or stayed stable. As the index on both dates initially increased past maximum instability seven days before the avalanches released, a stable index would have given optimal results. At other times, temperatures close to $-10°C$ for several days were observed between the LWC index peaking and avalanches releasing (figure 4.17). This could be cases were glide-snow avalanches release several days after water induced tensile cracks had formed. However, such cases are impossible for the LWC index to forecast.

Overall the LWC index does not predict wet-snow avalanche activity in times with high amounts of precipitation for a long duration. This could be an effect of how the shortwave radiation algorithm in the seNorge model assumes clear-sky radiation, which does not portray the real conditions on days with precipitation. On such days, the shortwave radiation is in reality reduced significantly with an increase in longwave radiation. The increase in longwave radiation might not make up for the large decrease in shortwave radiation, causing the modeled radiation to have a margin of error in such conditions that are much larger than in situations with clear skies. This can cause problems with how the LWC index rises and decreases in cloudy conditions.

5.4 Further Work

The current implementation of the LWC index into the seNorge model has weaknesses that are necessary to address before it can be reliably applied by forecasting services. In certain areas, the difference in elevation between adjacent grid cells was very large. This created scenarios where the LWC index was not calculated for the elevation where the avalanches were observed. A solution could be to run the seNorge model for an area with vertical gradients for both the temperature and precipitation. This would give indexes for the entire elevation range of a mountain, making it possible to see if the increased avalanche activity in a given elevation corresponds better with an LWC index with the exact same elevation.

It is likely that implementing a more precise cloud-fraction into the radiation equation will lead to more accurate radiation levels at times when precipitation is recorded. Such an implementation could be tested against the SNOWPACK model at Tyin if better precipitation records are available in the future. This would show the difference between modeled and observed radiation throughout the winter season in all types of weather. It would also show if the seNorge model can detect wet-snow avalanche activity for periods with precipitation as successfully as the SNOWPACK model.

Finally, at the current time, only observed weather data have been used to run the seNorge model. However, the approach allows for real forecasts of the LWC index by using numerical weather prediction data. This should be implemented to see if the index can reliably forecast periods with higher probability of wet-snow avalanche activity. Such an implementation would also be able to show us how often the index indicates high avalanche danger without any detection of avalanches, called false positives. Too many false positives is not desired in a forecasting perspective as people may become sceptical of the forecasts.

CHAPTER 6

Conclusion

In this thesis, we implemented a liquid water content index (LWC index) in the seNorge model to determine periods with high probability of wet-snow avalanche activity. This index has previously been implemented in Switzerland using the SNOWPACK model with decent results (Mitterer, Techel et al., 2013). We implemented the LWC index in the high-mountain version (v.2) of the seNorge model, which is an updated version of the currently operating seNorge model. This version has a more detailed formulation to calculate incoming solar radiation and can be updated as frequently as the SNOWPACK model, namely every three hours. Interpolated data from grid cells with a resolution of 1x1 km was used, making it possible to calculate the index for the entire mainland of Norway. The LWC index was tested against wet-snow avalanche activity in the regions around Tyin and Tromsø.

The results showed that specific meteorological conditions are required for the LWC index to be consistent with observed wet-snow avalanche activity. Times where the index increased due to typical spring conditions agreed well with wet-snow avalanche activity. In these cases, melt-water was caused by high temperatures without any precipitation, and during spring the modeled shortwave radiation was high. In such conditions, the onset of wet-snow avalanche activity was well detected. However, it was not possible to determine for how long the snowpack was unstable from the index. These results matched with the findings of Mitterer, Techel et al., 2013.

At times with several days of continuous precipitation, the LWC index did not properly indicate wet-snow avalanche activity. In such conditions, the index would rise at the wrong times, or even decrease, when wet-snow avalanche activity was observed. One possible cause could be that the algorithm used for calculating shortwave radiation in the seNorge model does not use any information about cloud cover. Instead, clear-sky radiation was always assumed, which does not portray the real conditions on days with precipitation. Another cause could be the inaccurate elevation of grid cells compared to that of the avalanches. In the model, a static temperature threshold was set for liquid or solid precipitation, and the temperatures were largely influenced by the elevation. If the elevation used in the model differs from the elevation of the avalanche, the model could misclassify the type of precipitation, causing the index to behave differently from what it would have at the correct altitude.

When implemented into the seNorge model, the LWC index still requires more work to reliably predict wet-snow avalanches. The current implementation only works at times when temperatures are rapidly increasing past 1°C and little to no precipitation is recorded. To be able to use this method in forecasting purposes, a solution for indicating wet-snow avalanche activity correctly at times with precipitation is necessary. In this thesis, the model was only run as nowcast, but the approach allows a real forecast using numerical weather prediction data. In further analyses, such data should be used as input for the seNorge model to assess if forecasts can be reliable.

Appendices

APPENDIX A

Figures and Tables

A.1 Tromsø Figures

A.1.1 2019

The two figures below shows the $\text{LWC}_{indexes}$ for grid cells on single mountains in 2019. The two mountains are the two farthest away from each other, with around 30 km separating them. One mountain has avalanches triggering on the east facing slope, while the other mountain have them triggering on south facing slopes.

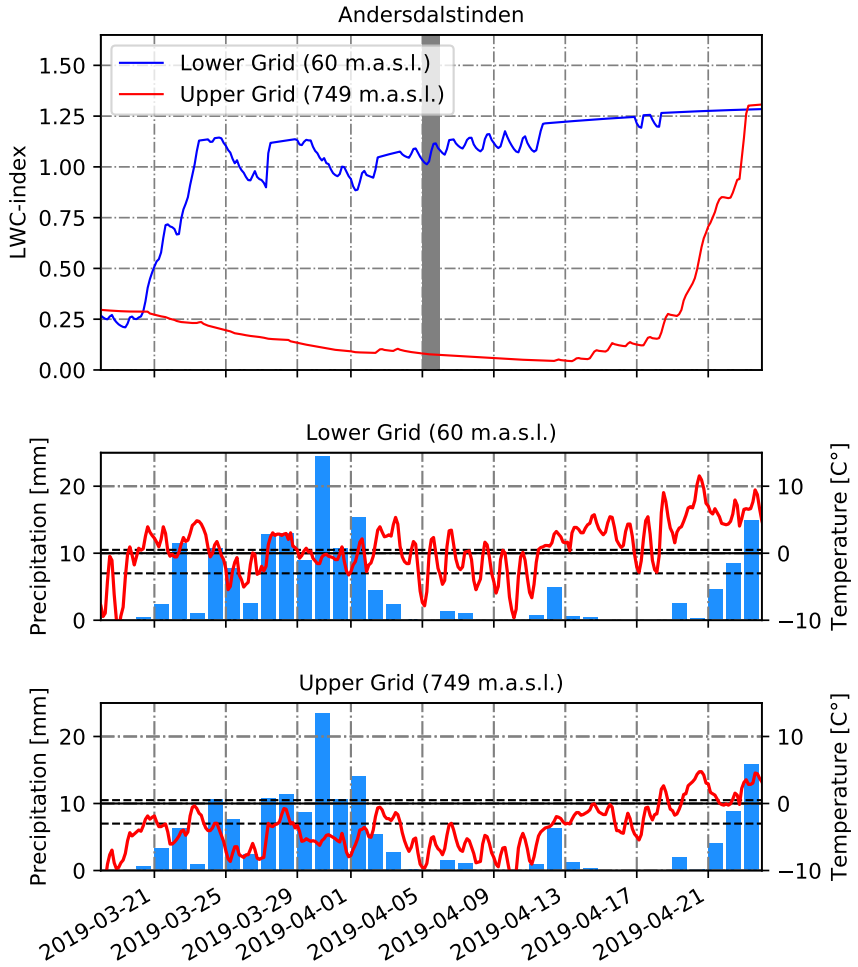

Figure A.1: 1) $\text{LWC}_{indexes}$ for the two grid cells on Andersdalstindens east facing slope around the avalanches in 2019. Possible time of onset for the avalanches are shown as grey bar.
2) The precipitation and temperature data for the two grid cells used to run the seNorge model. Daily summed precipitation is shown as blue bars, while temperature data is plotted every 3-hour in red lines. The two dotted black lines indicates the threshold air temperature for liquid or solid precipitation and possible temperature onset of melting in the model, on 0.5°C and -3°C respectively.

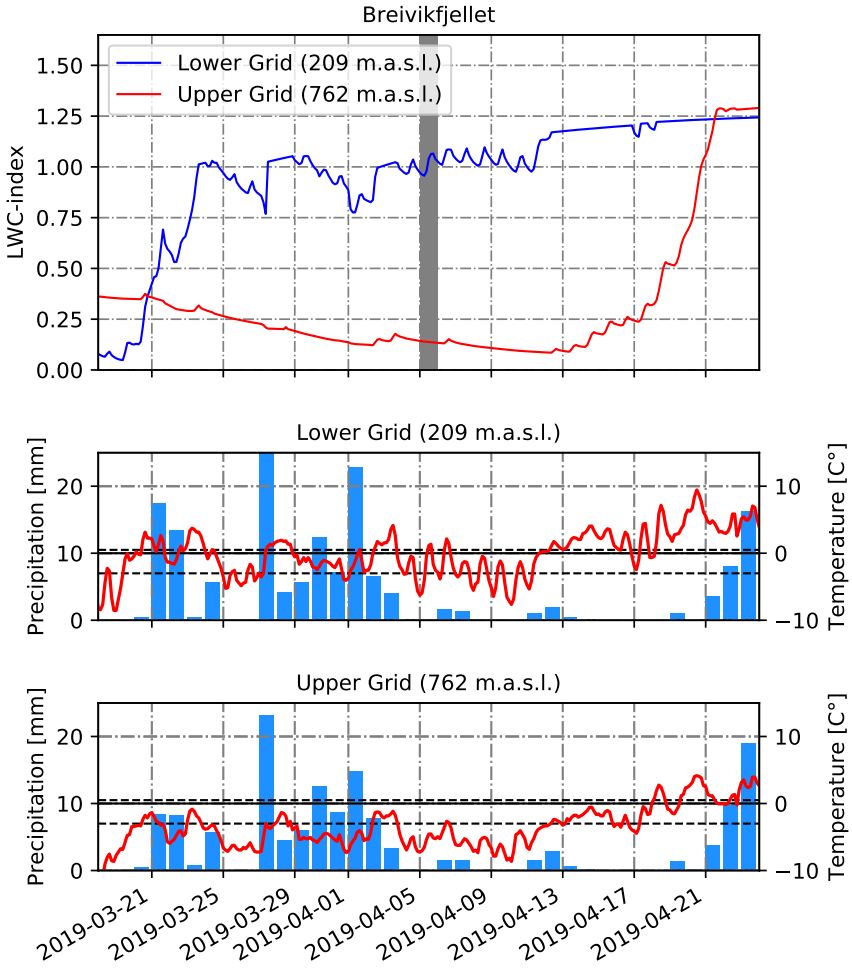

Figure A.2: 1) LWC$_{indexes}$ for the two grid cells on Breivikfjellets south facing slope around the avalanches in 2019. Possible time of onset for the avalanches are shown as grey bar.
2) The precipitation and temperature data for the two grid cells used to run the seNorge model. Daily summed precipitation is shown as blue bars, while temperature data is plotted every 3-hour in red lines. The two dotted black lines indicates the threshold air temperature for liquid or solid precipitation and possible temperature onset of melting in the model, on 0.5°C and -3°C respectively.

A.1.2 2015

The figure below shows the $\text{LWC}_{indexes}$ for the grid cells below 250 m.a.s.l. around the avalanches in May 2015.

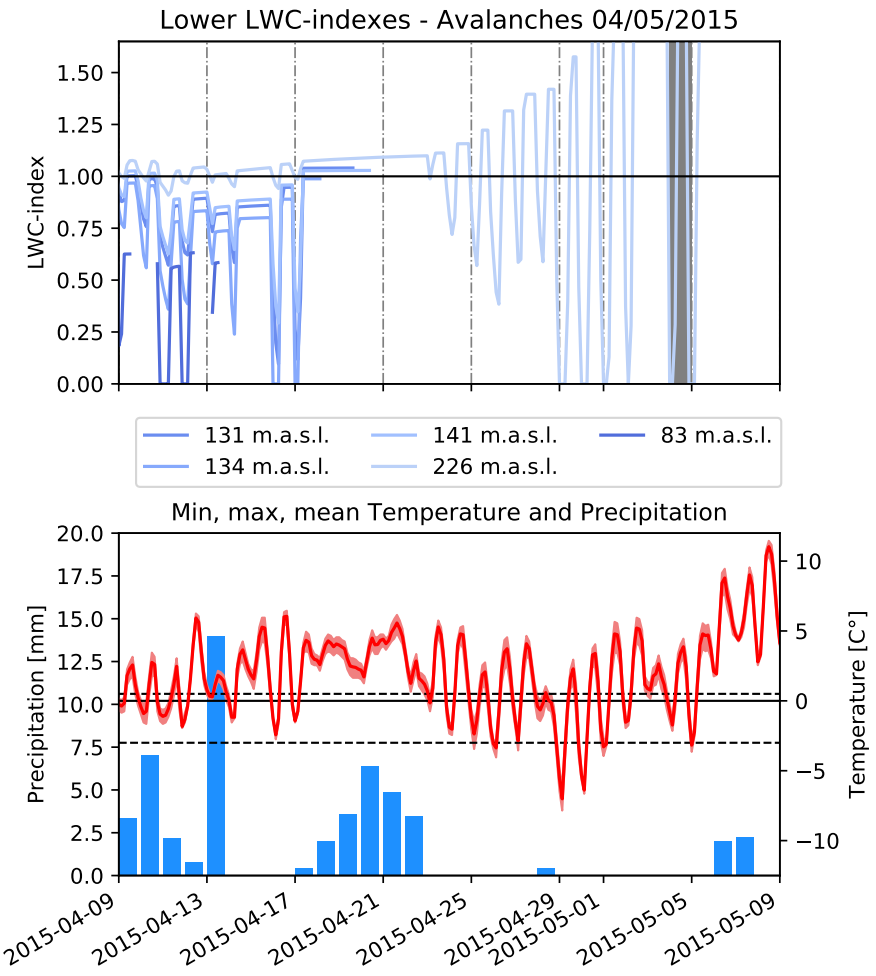

Figure A.3: 1) $\text{LWC}_{indexes}$ for the grid cells below 250 m.a.s.l. around the avalanches in May 2015. Possible time of onset for the avalanches are shown as grey bar.
2) The mean precipitation and minimum, maximum and mean temperature data for the grid cells used to run the seNorge model. Daily summed precipitation is shown as blue bars, while temperature data is plotted every 3-hour in red lines. The two dotted black lines indicates the threshold air temperature for liquid or solid precipitation and possible temperature onset of melting in the model, on 0.5°C and -3°C respectively.

Bibliography

Allen, R. G., Trezza, R. and Tasumi, M. (2006). 'Analytical integrated functions for daily solar radiation on slopes'. In: *Agricultural and Forest Meteorology* vol. 139, no. 1-2, pp. 55–73.

Armstrong, R. L. and Brun, E. (2008). *Snow and climate: physical processes, surface energy exchange and modeling*. Cambridge University Press.

Barfod, E., Müller, K., Saloranta, T., Andersen, J., Orthe, N. K., Wartianien, A., Humstad, T., Myrabø, S. and Engeset, R. (2013). 'The expert tool XGEO and its applications in the Norwegian Avalanche Forecasting Service'. In: *International Snow Science Workshop Grenoble*, pp. 282–284.

Bellaire, S., Herwijnen, A. van, Mitterer, C. and Schweizer, J. (2017). 'On forecasting wet-snow avalanche activity using simulated snow cover data'. In: *Cold Regions Science and Technology* vol. 144, pp. 28–38.

Bras, R. (1990). *Hydrology: An Introduction to Hydrologic Science*. Reading, Massachusetts: Addison-Wesley.

Bryn, A. and Potthoff, K. (2018). 'Elevational treeline and forest line dynamics in Norwegian mountain areas–a review'. In: *Landscape Ecology* vol. 33, no. 8, pp. 1225–1245.

Conway, H. and Raymond, C. (1993). 'Snow stability during rain'. In: *Journal of Glaciology* vol. 39, no. 133, pp. 635–642.

Denoth, A. (1980). 'The pendular-funicular liquid transition in snow'. In: *Journal of Glaciology* vol. 25, no. 91, pp. 93–98.

Engeset, R. V. (2013). 'National avalanche warning service for Norway–established 2013'. In: *Proceedings ISSW*, pp. 301–310.

Hock, R. (2003). 'Temperature index melt modelling in mountain areas'. In: *Journal of hydrology* vol. 282, no. 1-4, pp. 104–115.

Leppäranta, M. (1993). 'A review of analytical models of sea-ice growth'. In: *Atmosphere-Ocean* vol. 31, no. 1, pp. 123–138.

Lied, K. and Kristensen, K. (2003). *Snøskred: håndbok om snøskred*. Nesbru, Norway: Vett & Viten.

McClung, D. and Schaerer, P. A. (2006). *The avalanche handbook*. The Mountaineers Books.

Mitterer, C., Heilig, A., Schmid, L., Herwijnen, A. van, Eisen, O. and Schweizer, J. (2016). 'Comparison of measured and modelled snow cover liquid water content to improve local wet-snow avalanche prediction'. In: *International Snow Science Workshop Proceedings*.

Mitterer, C. and Schweizer, J. (2013). 'Analysis of the snow-atmosphere energy balance during wet-snow instabilities and implications for avalanche prediction.' In: *Cryosphere* vol. 7, no. 1.

Mitterer, C., Techel, F., Fierz, C. and Schweizer, J. (2013). 'An operational supporting tool for assessing wet-snow avalanche danger'. In: *Proceedings ISSW*. Vol. 33.

Pellicciotti, F., Brock, B., Strasser, U., Burlando, P., Funk, M. and Corripio, J. (2005). 'An enhanced temperature-index glacier melt model including the shortwave radiation balance: development and testing for Haut Glacier d'Arolla, Switzerland'. In: *Journal of Glaciology* vol. 51, no. 175, pp. 573–587.

Saloranta, T. M. (2012). 'Simulating snow maps for Norway: description and statistical evaluation of the seNorge snow model'. In: *The Cryosphere* vol. 6, no. 6, pp. 1323–1337.

Saloranta, T. M. (2016). 'Operational snow mapping with simplified data assimilation using the seNorge snow model'. In: *Journal of Hydrology* vol. 538, pp. 314–325.

Saloranta, T. M., Litt, M., Melvold, K. et al. (2016). 'Measuring and modelling snow cover and melt in a Himalayan catchment: instrumentation and model code setup in the Langtang catchment, Nepal. Lessons learned from the SnowAMP project.' In: *ICIMOD Working Paper*, no. 2016/10.

Saloranta, T. M., Thapa, A., Kirkham, J., Koch, I., Melvold, K., Stigter, E., Litt, M. and Møen, K. (2019). 'A model setup for mapping snow conditions in High-Mountain Himalaya'. In: *Frontiers in Earth Science* vol. 7, p. 129.

Tarboton, D. G., Luce, C. H. et al. (1996). *Utah energy balance snow accumulation and melt model (UEB), computer model technical description and users guide*. Citeseer.

Techel, F. and Pielmeier, C. (2009). 'Wet snow diurnal evolution and stability assessment'. In: *International Snow Science Workshop ISSW, Davos, Switzerland*. Vol. 27, pp. 256–261.

Trautman, S., Lutz, E., Birkeland, K. W. and Custer, S. G. (2006). 'Relating wet loose snow avalanching to surficial shear strength'. In: *Proceedings ISSW 2006*, pp. 71–78.

Vionnet, V., Brun, E., Morin, S., Boone, A., Faroux, S., Le Moigne, P., Martin, E. and Willemet, J. (2012). 'The detailed snowpack scheme Crocus and its implementation in SURFEX v7. 2'. In: *Geoscientific Model Development*, pp. 773–791.

Wolff, M., Isaksen, K., Petersen-Øverleir, A., Ødemark, K., Reitan, T. and Brækkan, R. (2015). 'Derivation of a new continuous adjustment function for correcting wind-induced loss of solid precipitation: results of a Norwegian field study'. In: *Hydrology and Earth System Sciences* vol. 19, no. 2, p. 951.

Yen, Y.-C. (1981). *Review of thermal properties of snow, ice, and sea ice*. Vol. 81. 10. US Army, Corps of Engineers, Cold Regions Research and Engineering Laboratory.